Holocene shifts in sub-surface water circulation of the North-East Atlantic inferred from Nd isotopic composition in cold-water corals

Quentin Dubois-Dauphin, Christophe Colin, Mary Elliot, Arnaud Dapoigny, Eric Douville

Holocene shifts in sub-surface water circulation of the North-East Atlantic inferred from Nd isotopic composition in cold-water corals

Quentin Dubois-Dauphin[1,2], Christophe Colin[1], Mary Elliot[3], Arnaud Dapoigny[4], Eric Douville[4]

[1]Laboratoire GEOsciences Paris-Sud (GEOPS), Univ. Paris-Sud, CNRS, Université Paris-Saclay, Rue du Belvédère, Bât. 504, 91405 Orsay, France.

[2]Now at Aix-Marseille Univ, CNRS, IRD, Coll de France, Centre Européen de Recherche et d'Enseignement des Géosciences de l'Environnement, Aix en Provence, France.

[3]Laboratoire de Planétologie/Géodynamique, UMR-CNRS 6112, Université de Nantes, Nantes, France.

[4]Laboratoire des Sciences du Climat et de l'Environnement, LSCE/IPSL, CEA-CNRS-UVSQ, Université Paris-Saclay, F-91191 Gif-sur-Yvette, France.

Abstract:

Variations of the Sub-Polar Gyre (SPG) and the Sub-Tropical Gyre (STG) circulation during the Holocene are believed to be related to regional and global climate over this time period. To improve our understanding of these phenomena we provide new constraints on variations in surface circulation patterns using neodymium isotopes (εNd) on precisely U-Th dated coral fragments of *L. pertusa.* The fragments were retrieved from two sediment cores taken from cold-water coral (CWC) mounds at ~ 127-134 m water depth in the Mingulay Reef Complex located on the Western British continental shelf. The results have been combined with εNd analyzed on seawater samples from two stations located on the continental shelf and margin in order to establish whether εNd is a reliable proxy of the ocean circulation variations and

notably of the relative contribution of water originating from the SPG and STG. εNd values in CWCs from the Mingulay Reef Complex range from -14.5±0.4 to -11.8±0.3, highlighting two major variations. Unradiogenic εNd values (-14.5±0.4) indicate a higher contribution of water from the SPG around 2.8 ka. Conversely, more radiogenic values at 3.4 ka (-11.8±0.3) point to a declining SPG strength, accompanied by stronger northward penetration of STG water along the western European margin transported by the Shelf Edge Current (SEC) and/or cooler and fresher waters from the interior Seas. The eastward extension of the SPG at 2.8 ka is associated with lower ^{14}C reservoir age (200 yrs) compared to periods associated with a higher contribution of STG waters. This indicates that ^{14}C reservoir ages are mainly a function of vertical mixing of the sub-surface of the ocean. As stronger vertical ventilation is not associated with a higher proportion of local radiogenic surface water, we hypothesize it could represent vertical ventilation in the North-Eastern Atlantic. Active SPG is associated with a better ventilation of the water masses within the SPG and warmer climatic conditions in Northern Europe and in the Eastern Norwegian Sea linked to an intensification of the surface limb of the AMOC.

Key words: Nd isotopic composition; cold-water corals; NE Atlantic; Sub-Polar Gyre

1. Introduction

The Atlantic Meridional Overturning Circulation (AMOC) transports warm saline surface water masses northwards and deeper cool waters southwards (Hansen and Østerhus, 2000; Read, 2001). The upper layer of the AMOC, the North Atlantic Current (NAC), loses much of its heat to the atmosphere on its way northwards, impacting the climate over Europe (Hall and Bryden, 1982). Whereas variability of the lower branch of the AMOC is relatively well established during the Holocene, at least for the Iceland-Scotland Overflow Water (ISOW)

and the Labrador Sea Water (LSW) (e.g. Hillaire-Marcel et al., 2001; Hoogakker et al., 2011; Thornalley et al., 2013; Mjell et al., 2015), the variations of the upper layer of the AMOC are not yet well established. This is due to the complex spatial and temporal variability of the classical Sea Surface Temperature (SST) and Sea Surface Salinity (SSS) proxies used to track past changes of the AMOC that are strongly influenced by an orbitally-induced insolation trend and the final disintegration of the residual Laurentide ice sheet during the early Holocene, which induces a pronounced provincialism in the surface physical property records of the North Atlantic (e.g. de Vernal and Hillaire-Marcel, 2006; Renssen et al., 2009).

It has been suggested that during modern times variations in the shape and position of the subpolar gyre (SPG) (Fig. 1) play a major role in the redistribution of fresh melt-water and in pole-ward heat transport at surface and intermediate depths and subsequently have an impact on the AMOC strength and the properties of waters entering the Nordic Seas (e.g. Häkkinen et al., 2013). The NAC follows the boundary between the North Atlantic subpolar gyre (SPG) and the subtropical gyre (STG), and its position, intensity and composition have been modulated by SPG variations over recent decades (Hàtun et al., 2005; Berx and Payne, 2017; Zunino et al., 2017). Foukal & Lozier (2018), by using a combination of empirical orthogonal functions and direct calculations of the size and strength of the SPG, have proposed that the SPG dynamics may not control the magnitude of the STG waters flowing into the North east Atlantic, on interannual time scales. However, numerous paleohydrological records point to a major role of the SPG on longer time scales (see references below). During the early Holocene, a reorganization of the mid-depth (200-800 m) circulation has been highlighted at about 7-6 ka, with a weakened SPG leading to a stronger northward penetration of temperate water masses in the North-East Atlantic (Thornalley et al., 2009; Colin et al., 2010). Other studies based on cold-water corals from the Bay of Biscay and the Rockall Trough have highlighted an existing link between SPG intensity and the North Atlantic Oscillation (NAO),

74 i.e. atmospheric circulation (Copard et al., 2012; Montero-Serrano et al., 2013). Between 1950
75 and 1990, periods characterized by a dominant negative phase of NAO were associated with a
76 stronger influence of mid-depth STG water (Montero-Serrano et al., 2013). Over the last 1500
77 yrs, the warm Medieval Climatic Anomaly (between 1000 AD and 1250 AD), characterized
78 by a persistently positive NAO phase, resulted in greater eastward extension of the mid-depth
79 SPG in the North Atlantic (Copard et al., 2012). Conversely, the Little Ice Age (between 1350
80 AD and 1850 AD), characterized by a persistently negative NAO phase, is associated with the
81 westward contraction of the mid-depth SPG (Copard et al., 2012). Overall, these records have
82 shown that Holocene climatic anomalies are associated with mid-depth SPG dynamics which
83 are in turn affected by changes in wind stress and/or freshwater input from the Labrador Sea
84 (Thornalley et al., 2009; Colin et al., 2010; Copard et al., 2012). Subsequent variations in the
85 heat and salt budgets at intermediate depths may have contributed to changes in the properties
86 of North Atlantic inflow to the Nordic Seas and thus to deep-water formation.

87 The Mingulay Reef Complex, located on the Western British continental shelf (Fig. 1), is a
88 potential target to track past changes of the SPG extension using the εNd proxy because it
89 receives waters from the NAC. In addition, cold-water corals (CWCs) have been shown to act
90 as useful archives for identifying rapid changes in the dynamics of water masses (Lutringer et
91 al., 2005; Colin et al., 2010; van de Flierdt et al., 2010; Copard et al., 2010, 2012; Montero-
92 Serrano et al., 2013; Wilson et al., 2014; Chen et al., 2015; Dubois-Dauphin et al., 2016;
93 Douarin et al., 2016). Firstly, their aragonitic skeleton can be precisely dated thanks to U-
94 series disequilibrium methods (Adkins et al., 1998; Cheng et al., 2000; Douville et al., 2010).
95 Secondly, they do not suffer from the same problems often encountered in marine sediment
96 cores, which are often affected by bioturbation, smoothing the original signals, and which are
97 characterized by low sedimentation rates that limit our ability to obtain records with
98 centennial resolutions. Furthermore, the Nd isotopic composition, expressed as εNd =

99 ([($^{143}Nd/^{144}Nd)_{sample}/(^{143}Nd/^{144}Nd)_{CHUR}$] − 1) × 10000 (CHUR: Chondritic Uniform Reservoir
100 [Jacobsen and Wasserburg, 1980]), of living and fossil scleractinian CWCs faithfully traces
101 water mass provenance and mixing in the ocean (e.g. van de Flierdt et al., 2010; Copard et al.,
102 2012; Struve et al., 2017). Taking into consideration that mid-depth STG and SPG water
103 masses are characterized by contrasted Nd isotopic signatures (εNd ≈ -10 and εNd≈ -15,
104 respectively; Lambelet et al., 2016; Dubois-Dauphin et al., 2017), CWC εNd records obtained
105 previously in the Rockall Trough and in the northern Bay of Biscay have been used to
106 reconstruct the eastward extension of the mid-depth SPG (Colin et al. 2010; Copard et al.,
107 2012; Montero-Serrano et al., 2011, 2013).

108 In this paper we present a high-resolution εNd record for the last 4500 yrs, which is derived
109 from CWCs from the Mingulay Reef Complex, located at the sub-surface under the strong
110 influence of NAC water. Our objective is to track hydrological changes in the SPG dynamics
111 during the Holocene. Ambient seawater εNd was also investigated to assess seawater εNd of
112 the Western British continental shelf and margin and to verify that εNd is a reliable proxy for
113 tracking past changes in the influence of the SPG in this region. This CWC εNd record was
114 compared to previously published $\Delta^{14}C$ performed by Douarin et al. (2016) that was
115 interpreted in terms of changes in water mass origin. It also complements well previous
116 studies based on εNd in the Rockall Trough (Colin et al., 2010; Copard et al., 2012) that have
117 highlighted major variations of the mid-depth SPG dynamics throughout the Holocene. Our
118 study permits us to re-interpret $\Delta^{14}C$ with a proxy of water mass origin and provides new
119 evidence of abrupt changes in the composition of water masses entering the Nordic Seas;
120 these changes are linked to variations in the shape and strength of the SPG.

121

122 **2. Hydrological setting**

123 Presently, the deepest waters (>100 m) and the waters overlying the outer parts of the shelf of
124 west Scotland are of Atlantic origin (Inall et al., 2009). At the surface, the northward flowing
125 Scottish Coastal Current (SCC) brings cooler and fresher waters from the Irish and Clyde
126 Seas (Ellett and Edwards, 1983) (Fig. 1). The Mingulay Reef Complex (56°50'N; 7°20′W;
127 100-260 m water depth) is thus primarily bathed by Atlantic water (Dodds et al., 2007). The
128 upper-layer Atlantic water off the Mingulay Reef Complex, carried by the NAC, results from
129 the mixing of saline Eastern North Atlantic Central Water (ENACW) originating from the
130 Bay of Biscay (Ellett and Martin, 1973; Ellett et al., 1986; Pollard et al., 1996) and the fresher
131 Modified North Atlantic Water (MNAW) originating in the North-West Atlantic (New and
132 Smythe-Wright, 2001). The MNAW is formed by the mixing of the Western North Atlantic
133 Central Water (WNACW), which flows from the Caribbean Sea, with the Sub-Arctic
134 Intermediate Water (SAIW). The SAIW is characterized by low temperatures and salinity and
135 is formed in the upper layers of the southern Labrador Sea (Arhan, 1990). Both WNACW and
136 SAIW are transported north-eastwards into the NAC where vertical mixing occurs (Arhan,
137 1990). The NAC is composed of three main branches (Daniault et al., 2016). The northern and
138 central branches bifurcate west of the Rockall Trough and feed the cyclonic circulation in the
139 Iceland Basin and the Irminger Sea (Fig. 1). The southern branch penetrates into the Rockall
140 Trough (Fig. 1)

141 All along the European margin, the Shelf Edge Current (SEC) forms a northward-flowing
142 boundary current that brings warm and saline upper water with ENACW characteristics
143 through the Rockall Trough and the Scottish margin (Hill and Mitchelson-Jacob, 1993; White
144 and Bowyer, 1997; Holliday et al., 2000) (Fig. 1). Below this, the Mediterranean Sea Water
145 (MSW) flows northwards from the Gulf of Cadiz with a main core located at 1000-1200 m
146 water depth. Nevertheless, the MSW cannot be traced through εNd, salinity and potential
147 temperature at mid-depth further north than the Porcupine Seabight (Iorga and Lozier, 1999;

148 McCartney and Mauritzen, 2001; New and Smythe-Wright, 2001; Lavender et al., 2005;
149 Dubois-Dauphin et al., 2017).

150 The NAC strength, direction and composition respond to SPG dynamics (Hátún et al., 2005):
151 when the SPG circulation is stronger and presents a more pronounced east–west shape the
152 SPG water influence on the NAC is increased relative to the STG water, coupled with a strong
153 AMOC. Conversely, when the SPG circulation is weaker and forms a more pronounced
154 north–south shape, a lower contribution of SPG water flows to the NW European Margin
155 relative to the STG water (Larsen et al., 2012; Hansen et al., 2015).

156

157 ## 3. Material and methods

158 ### 3.1.1. CWC samples

159 This study has investigated 23 well-preserved fossil CWCs of the species *Lophelia pertusa*,
160 collected in two cores from the Mingulay Reef Complex located on the Western British
161 continental shelf (Fig. 1 and Table 1). The cores, +56-08/929VE (56°49′19″N - 7°23′27″W,
162 127 m water depth) and +56-08/930VE (56°49′20″N -7°23′47″W, 134 m water depth), were
163 collected in October 2007 by the British Geological Survey during a survey (Cruise 15) on
164 board of the NERC vessel RRS James Cook (Stewart and Gatliff, 2008) (Table 1). The coring
165 sites are located within 300 m of each other at quite a similar water depth on small carbonate
166 mounds of the Mingulay Reef Complex (Figure 1; Table 1). The sediment cores are
167 composed of biogenic fragments (mainly CWC fragments) in a carbonate matrix. Three
168 additional surface videograb samples (GRAB 15.5.5.10; GRAB 56.08.928 ; GRAB 1151)
169 were retrieved from the seafloor with a Remotely Operated Vehicle close to the location of
170 the cores (see location in Fig. 1 and Table 1).

U-Th ages obtained for CWC samples collected in the Mingulay Reef Complex were published by Douarin et al. (2016) (Table 1). They document three major peaks in growth rate that are centered at 3.7, 4, and 4.2 ka BP. Two major reductions in growth rate were observed at 1.75–2.8 ka and 3.2–3.6 ka BP. The coral fragments investigated in this study, from cores +56-08/929VE and +56-08/930VE, range between 4.29±0.26 and 2.09±0.018 ka BP (Table 1). In addition, GRAB 56.08.928, GRAB 1151 and GRAB 15.5.5.10 samples have been dated to 2.67±0.014, 1.31±0.011 and 0.02±0.013 ka BP, respectively (Table 1).

3.1.2. Seawater samples

During the R/V Atalante MINGULAY-ROCKALL cruise in June 2016, 12 seawater samples were collected at 2 full water column stations MR-4 (56°37.44' N; 9°5.48' W) and MR-5 (56°46.04'N; 7°25.98' W) (Fig. 1, Table 2). These samples, located on the Western British continental shelf (station MR5) and margin (station MR4), were collected in order to assess seawater εNd flowing around the Mingulay Reef Complex. The seawater samples and water column hydrographic parameters (temperature and salinity) were collected using a CTD-Rosette system equipped with 12 10-liter Niskin bottles and a standard Sea-Bird SBE 911plus CTD-Rosette system. The samples were then filtered through 0.8-0.45 µm AcroPak 500 capsule filters and transferred to 10-liter acid-cleaned bottles, and immediately acidified to a pH of 2 using suprapur 2 N HCl.

3.2.3 Analytical procedures for Nd isotope measurements

Each coral fragment used in this study corresponded to one polyp of the *Lophelia pertusa* species, integrating only a few years of growth (Freiwald et al, 2004; Sabatier and al., 2012a). The CWC samples were subjected to a mechanical and chemical cleaning procedure (Copard et al., 2010). The visible contaminations, such as Fe-Mn coatings and detrital particles, were carefully removed from the inner and outermost surfaces of the coral skeletons using a small

diamond blade. The physically cleaned fragments were ultrasonicated for 10 min. with 0.1 N ultra-clean HCl, followed by several MilliQ water rinses and finally dissolved in 2.5 N ultraclean HNO_3. Neodymium was separated from the carbonate matrix using Eichrom TRU and LN resins, following the analytical procedure described in detail in Copard et al. (2010).

Neodymium was purified from seawater samples following the analytical procedures described in detail by Lacan and Jeandel (2001) and Wu et al. (2015). Briefly, seawater REEs were preconcentrated using SepPak Classic C18 cartridges loaded with a HDEHP/H2MEHP complexing agent. Solutions were then passed through a cationic resin (AG50W-X8) and finally Nd was extracted and purified using an Eichrom Ln-Spec resin following the method described in detail by Copard et al. (2010). This purification process and the measurement techniques applied follow approved GEOTRACES protocols and GEOPS laboratory participated in the international GEOTRACES intercalibration study (van de Flierdt et al., 2012).

The $^{143}Nd/^{144}Nd$ ratios of seawater samples and of the CWCs from the Mingulay Reef Complex, were analyzed using a Thermo Scientific Neptune Plus MC-ICPMS installed at the Laboratoire des Sciences du Climat et de l'Environnement (LSCE, Gif-sur-Yvette, France). The mass-fractionation correction was made by normalizing $^{146}Nd/^{144}Nd$ to 0.7219 by applying an exponential-fractionation correction. During the analytical sessions, every two samples were bracketed with analyses of appropriate standard JNdi-1 and La Jolla Nd solutions, which are characterized by certified values of 0.512115±0.000006 (Tanaka et al., 2000) and 0.511858±0.000007 (Lugmair et al., 1983), respectively. Standard JNdi-1 and La Jolla solutions were analyzed at concentrations similar to those of the samples (4-10 ppb). The external reproducibility (2σ) deduced from repeated measurements of the La Jolla standard and JNdi-1, ranged from 0.2 to 0.4 Epsilon units for the different analytical sessions. The

analytical error associated with each sample analysis is taken as the external reproducibility of the La Jolla standard for each session.

4. Results

4.1. Seawater samples

The Nd isotopic compositions of the seawater samples from stations MR-4 and MR-5 are provided in Table 2 and Figure 2. Station MR-5 is located on the continental shelf, very close to the Mingulay Reef Complex. At station MR-5, εNd values decrease downward from -11.6±0.2 at the surface to -13.1±0.3 at a water depth of 240 m (Fig. 2). Temperature decreases from 12 to 9.5°C between depths of 30 and 80 m, then remains constant (9.5°C) down to 240 m water depth (Fig. 2). Conversely salinity increases from 34.5 to 35.2 in the upper 100 m, then displays a constant value of 35.2 down to 240 m water depth (Fig. 2).

On the other hand, station MR-4 was collected on the continental slope. Seawater samples from station MR-4 exhibit similar εNd values at all depths, within the error bars, centered around -14 from the surface to 540 m water depth (Fig. 2). Temperature decreases from 13 to 10 °C between depths of 20 and 80 m, then displays a constant value of about 9.7°C down to 550 m water depth. Salinity displays an almost constant value of about 35.3. The upper 50 m are, however, slightly less saline (Fig. 2).

4.2. Cold Water Coral samples

Overall, CWC εNd values from the Mingulay Reef Complex range from -14.5±0.4 to -11.8±0.3 (Fig. 3). The earlier part of the record (4.5 – 3.5 ka) displays a narrow range of values between -13.1±0.3 and -12.5±0.3 (Fig. 3). An abrupt increase of the εNd values for corals occurred between 3.40 and 3.20 ka BP, reaching between -12.1±0.3 and -11.8±0.3 (Fig.

242 3). A return to lower values (-13.1±0.3 to -12.4±0.4) is observed between 3.12 and 2.82 ka
243 BP, followed by an abrupt and short decrease over 100 years to -14.5±0.4 at 2.75 ka BP (Fig.
244 3). After 2.67 ka BP, only four specimens display εNd values from -12.0±0.4 to -13.2±0.5
245 (Fig. 3).

246

247 **5. Discussion**

248 *5.1. Significance of the εNd record*

249 The youngest CWC sample collected in the Mingulay Reef complex, with a modern age of
250 0.02±0.013 ka BP (Douarin et al., 2016), displays an εNd value of -13.2±0.5 (Fig. 3) which is
251 similar, within the error bars, to the present-day value of seawater flowing at depth of the
252 study site (between -12.9±0.2 and -12.4±0.2 at 101-152 m water depth; station MR-5) (Fig. 2
253 and 3). At station MR-4, located on the continental slope, seawater samples values range from
254 -14.4±0.2 to -13.8±0.2 down to 500 m water depth (Fig. 2). These values are in agreement
255 with seawater analyzed in the Rockall Trough (ICE-CTD 03; Dubois-Dauphin et al., 2017)
256 the values of which range from -14.0±0.2 to 13.3±0.2 for the same depth interval (Fig. 4),
257 implying that subsurface water masses brought by the NAC have a strong influence along the
258 continental slope near the study site. In contrast, station MR-5, located on the continental
259 shelf, exhibits more radiogenic values at all depths compared to the continental slope (MR-4)
260 and the Rockall Trough (ICE-CTD 03; Dubois-Dauphin et al., 2017). The εNd value of warm
261 and saline surface water (upper ENACW) flowing in the SEC is poorly constrained along the
262 European margin. It has been reported to be radiogenic in the Bay of Biscay (-10.7±0.3 at 140
263 m in CAROLS stations; Copard et al., 2011), while there are no values shallower than 400 m
264 published for the Porcupine Seabight (-13±0.2 at 400 m in station ICE-CTD 02; Dubois-
265 Dauphin et al., 2017) (Fig. 4). This radiogenic water brought by the SEC is expected to have a
266 strong influence on the Mingulay Reef Complex as seen at station MR-5.

Nevertheless, Nd isotopic signatures for the SCC that circulates from the Irish Sea and the Firth of Clyde are unknown. However, rocks and river sediment samples from the northern British Isles display a mean εNd value of -10.6 ± 0.4 (Davies et al., 1985), suggesting a rather radiogenic Nd isotopic signature for seawater from interior Seas. Crockett et al. (2018) have provided Nd concentrations (20 to 60 $pmol.kg^{-1}$) from seawater collected in a coastal station (station 9G, 166 m bottom depth; Fig. 1) located close to the Mingulay Reef Complex suggesting possible local desorption from resuspended sediments or pore water release to the overlying water column. Seawater εNd obtained in the upper 50 m of the MR-5 water station, collected above the Mingulay Reef Complex, allows us to establish for the first time the εNd value of seawater flowing along the Scottish margin; this value is around -11.7±0.2 and is associated with a temperature and salinity of about 10-12°C and 34.5-34.9, respectively (Fig. 2). This suggests that surface water is likely affected by local inputs from the Scottish shelf and/or the interior Seas. On the other hand, the εNd values are more unradiogenic (from -13.0±0.3 to -12.4±0.2) below 100 m at water station MR-5 (in the range of Porcupine Seabight; Dubois-Dauphin et al., 2017) and associated with salinity of ~35.2 suggesting that CWCs from the Mingulay Reef Complex are under the influence of a mixing between SEC and NAC waters. Furthermore, the initial $\delta^{234}U$ values of the samples considered in this study ranged from 142.9 ± 2.4 to 150.0 ± 3.5 (2σ uncertainties; Douarin et al., 2013), which is in the range of the modern seawater value (146.8±0.1; Andersen et al., 2010), while ^{232}Th values for all corals were low (<0.48±0.07 ppb; Douarin et al., 2013). These arguments do not support an influence of a local source on CWC εNd from the Mingulay Reef Complex. However, the desorption from resuspended sediments cannot be ruled out.

εNd of CWC samples, collected at 747 m water depth at the SW Rockall Trough margin, has been investigated by previous studies and has been shown to range from -11.9±0.3 to -14.4±0.2 over the last 4500 yrs (Colin et al., 2010 ; Copard et al., 2012) (Fig. 3). These values

292 are close to those obtained at the Mingulay Reef Complex, with a generally good
293 correspondence between samples of the same age in both sites (Fig. 3). Seawater εNd
294 investigated in the Rockall Trough does not indicate significant variations of Nd isotopic
295 composition down to 1000 m water depth (-13.3±0.2 to -14.0±0.2; Dubois-Dauphin et al.,
296 2017) and presents similar values to those found at station MR-4 (Fig. 4). This implies a
297 relatively strong homogeneity of the Nd isotopic composition of the surface-to-mid water
298 masses of the Rockall Trough. On the other hand, station MR-5 displayed more radiogenic
299 values, as the Mingulay Reef Complex is likely to experience a strong mixing with STG
300 water. Nevertheless, both sites should be under the influence of the gyre circulation system. In
301 this instance, it is therefore possible to consider that the CWCs from the shallow Mingulay
302 Reef Complex record similar gyre dynamics than the mid-depth of the SW Rockall Trough
303 margin.

304 The εNd record from the Rockall Trough provides evidence of negative excursions during the
305 warm Medieval Climatic Anomaly (between 1000 AD and 1250 AD) and during the most
306 recent period (1950 AD to 2000 AD) (Fig. 3), which have been interpreted as indicating a
307 strengthened SPG and an increase in the subpolar water contribution to the Nordic Seas
308 (Copard et al., 2012). CWCs from the Mingulay Reef Complex do not record these events as
309 none of the sample ages match these periods. However, they indicate another major negative
310 excursion of εNd values at about 2.8 ka BP (Fig. 3).

311 The presence of Ice Rafted Debris (IRD) during the Holocene is evidenced in North Atlantic
312 sediment cores located in the Rockall Trough (cores MC52 and VM29-191; Bond et al., 2001)
313 (Fig. 1) by peaks in hematite-stained grains and Icelandic glass. It has been shown to have a
314 potential influence on εNd records during periods of northern-hemisphere ice sheet collapse
315 throughout the MIS2, due the input of very radiogenic volcanic material (Roberts and
316 Piotrowski, 2015). However, the Holocene is not marked by such variations in the Nd isotopic

317 signature of water masses (Roberts and Piotrowski, 2015). In addition, the εNd records
318 extracted from CWCs of the Mingulay Reef Complex (this study) and the Rockall Trough
319 (Colin et al., 2010) do not seem to be affected by this mechanism, at least not during the late
320 Holocene, as an increase in Icelandic glass concentration in the Rockall Trough (0.1-0.6 ka,
321 1.2-1.5 ka, 2.8-2.9 ka, 3.3-3.4 ka, 4.0-4.1 ka; Bond et al., 2001) is not linked to systematically
322 higher εNd values. Overall, a strong contribution of Nd input from volcanic material can
323 probably be excluded, suggesting that CWCs from the Mingulay Reef Complex record εNd
324 variability in the mixing between SEC and NAC water through time.

325 Fresh sub-surface water flowing into the SPG is characterized by unradiogenic εNd values (-
326 14 to -16) while subtropical water exhibits more radiogenic values (-10 to -12) (Lacan &
327 Jeandel, 2004, 2005; Lambelet et al., 2016; Dubois-Dauphin et al., 2017). It has been shown
328 that εNd of the NAC was dominated by the subpolar gyre signature due to higher Nd
329 concentrations in the subpolar surface waters compared to the northern subtropical gyre
330 waters (Lambelet et al., 2016; Dubois-Dauphin et al., 2017). Therefore, when the subpolar
331 gyre extension is enhanced, NAC seawater is expected to be even more unradiogenic than
332 today. Conversely, during times of westward contraction of the subpolar gyre, a stronger
333 influence of temperate subtropical water flowing northwards along the European margin
334 could increase the εNd value at the study site. εNd record of the Mingulay Reef Complex can
335 be associated to the spatial evolution of the interface between the SPG waters and the
336 ENACW carried northwards by the SEC. Thus, lower εNd recorded (2.8 ka) in the subsurface
337 Mingulay Reef Complex may reflect periods of intense, eastward extension of water from the
338 SPG, while higher εNd (3.4 ka) should point to a westward contraction of the SPG and a
339 subsequent stronger influence of the STG waters carried by the slope current and/or water
340 from interior Seas.

341 *5.2.Hydrological and climate implications of Nd isotope variations*

342 U-series dating and radiocarbon ages (Douarin et al., 2016) have been obtained for CWC
343 samples from the Mingulay Reef Complex investigated in this study, thereby allowing us to
344 calculate $\Delta^{14}C$ of the water (Douarin et al., 2016) so as to track changes in the circulation of
345 sub-surface water masses during the Holocene. The Marine Reservoir Effect (MRE) of the
346 NAC and derived branches averages about 400 years (Stuiver et al., 1998). However, the
347 fresher water flowing into the SPG is depleted in radiocarbon compared to the NAC,
348 displaying a MRE between 450 and 500 years (Eiríksson et al., 2011; Franke et al., 2008).
349 Along the western European margin, in the inter-gyre area, the mean MRE for sub-surface
350 water has been estimated at 380±60 years (Tisnerat-Laborde et al., 2010). Consequently, high
351 MRE in the Mingulay CWCs has been interpreted as indicating a stronger influence of
352 subpolar water (Douarin et al., 2016), linked to the extension of the SPG (Hatun et al., 2005).

353 The εNd record obtained in this study co-varies with the reconstructed MRE values for the
354 Mingulay CWCs (Douarin et al., 2016), as older (younger) MRE is synchronous with more
355 (less) radiogenic εNd (Fig. 5). At 3.4, the coral εNd record shifts towards more radiogenic
356 values (~ -11.8) associated with an increase in MRE (up to 592±41 years). Conversely, low
357 MRE values (down to 207±38 years) occur at about 2.8 ka and are associated with more
358 unradiogenic values (~ -14.5) (Fig.3 and 5).

359 As STG water exhibits more radiogenic values than water flowing in the SPG (see section
360 5.1), a shift toward more radiogenic εNd values at Mingulay points to a weakened SPG,
361 promoting the northeastward advection of subtropical water to the Rockall Trough and the
362 Mingulay Reef Complex. This conclusion is inconsistent with the previous interpretation of
363 MRE variations in Mingulay corals (Douarin et al., 2016). Alternatively, MRE variations
364 could be interpreted as changes in gas exchange rates between the atmosphere and the surface
365 mixing layer (Ascough et al., 2009; Tisnérat-Laborde et al., 2010; Wanamaker et al., 2012). A
366 homogenization of the water column due to enhanced wind stress could result in a younger

MRE from Mingulay corals, as previously observed in CWCs from the Bay of Biscay (Montero-Serrano et al., 2013). Previous studies have shown that downwelling phenomena occur at the Mingulay Reef Complex (Davies et al., 2009). A long-term influence of downwelling on the area of the Mingulay Reef Complex should have resulted in the transfer of rather radiogenic εNd surface waters (-11.7±0.2, station MR-5) to depth at times of lower MRE. However, this is not the case as εNd from Mingulay CWCs decreases when the marine age reservoir is low (i.e. at 2.8 ka) and inversely (i.e. at 3.4 ka). Similarly, inputs of Scottish fjords and coastal waters, which are likely to result in reduced regional MRE (Stuiver and Braziunas 1993) and higher εNd values (Davies et al., 1985), are not supported by the data trend from Mingulay CWCs. Furthermore, a moderate regional deviation in marine reservoir age (-26±14 years) has been estimated for the Interior Seas (Cage et al., 2006), suggesting a limited influence on radiocarbon variations. Finally, the influences of ^{14}C-deficient carbon derived from humus or carbonate bedrock are likely to be small (Cage et al., 2006). Taken together, all the above evidences suggest that MRE variations recorded in the Mingulay Reef Complex are the result of changes in vertical mixing occurring in the NAC and/or SEC and that the source of the young MRE anomaly should be water of subpolar origin.

The more radiogenic εNd value between at 3.4 ka, associated with high MRE, is synchronous with storminess maxima recorded in Icelandic eolian soil deposits (Jackson et al., 2005) (Fig. 6). On the basis of several paleostorm activity records, five Holocene storm periods have been defined in the North-East Atlantic during the mid- to late Holocene (5.8-5.5 ka; 4.5-3.9 ka; 3.3-2.4 ka; 1.9-1.05 ka and 0.6-0.25 BP) with a frequency of about 1,500 years (Sorrel et al., 2012). These storm periods have been shown to coincide with an enhanced upper-water-column stratification south of Iceland and increases in temperature and salinity (Sorrel et al., 2012). Enhanced stratification and changes in eastern Atlantic water properties are consistent with a westward contraction of the SPG accompanied by a stronger northward penetration of

warm and saline waters of the STG (Sorrel et al., 2012). In addition, a decrease in the temperature gradient of the North Atlantic has been linked to a southward shift of the westerlies and low-pressure systems, leading to southward displacement of the storm tracks along the European coasts (Sabatier et al., 2012b; Sorrel et al., 2012). These observations on a multi-millenial timescale are consistent with centennial variations occurring at the Mingulay Reef Complex. Hence, we propose the εNd maximum recorded in the Mingulay Reef Complex at 3.4 ka, coeval with strong storms activity (Fig. 6), indicates a stronger influence of subtropical water in the NAC, leading to a higher stratification of the water column in agreement with older MRE (Fig. 6 and 7).

Conversely, the minimum εNd value at 2.8 ka, which is in phase with a younger MRE, is not associated with strong storm activity (Fig. 6). It is, however, characterized by periods of elevated Na^+ in the Greenland Ice Sheet Project 2 (GISP2) ice core which are interpreted as sea salt transported by strengthened westerly winds (O'Brien et al., 1995; Mayewski et al., 2004; Jackson et al., 2005) (Fig. 6). Consequently, increased wind intensity at high latitudes of the North Atlantic results in an extension of the SPG leading to more unradiogenic εNd values and lower MRE in the Mingulay Reef Complex (Fig. 7).

The variability in north Atlantic gyre circulation could in turn impact the AMOC dynamics (Oppo et al., 2003; Thornalley et al., 2009). High temporal resolution sea surface temperature (SST) reconstructions for the late Holocene have been investigated in the Nordic Seas (core MD99-2275, Sicre et al., 2008). SST variability in the North-East Atlantic and the Nordic Seas has a strong influence on colder and warmer climate over Europe. Copard et al. (2012) have demonstrated that coral εNd shifted towards values indicative of a stronger SPG during the Medieval Climatic Anomaly and a weaker SPG during the Little Ice Age. Similarly, the 2.8 ka event recorded in CWCs from the Mingulay Reef Complex is coeval with a temperature maximum in the Nordic Seas, while lower SSTs are associated with the 3.4 ka

event (Sicre et al., 2008) (Fig. 6). These findings are in agreement with a previous study that shows a linkage between LSW formation, SPG strength and climate periods in North-West Europe (Moffa-Sanchez and Hall, 2017). In addition, the lower εNd from subtler variations of the Mingulay corals are often associated with higher temperatures north of Iceland (see dashed lines in Fig. 6). We conclude that an extension (contraction) of the SPG and the subsequent intensification (weakening) of the AMOC results in a higher (lower) latitudinal heat flux in the North-East Atlantic and the Norwegian Seas (Fig. 7), as has been evidenced during the last millennium (Wanamaker et al., 2012). By comparing SST variability in the Nordic Seas and the subpolar Atlantic, Miettinen et al. (2012) have demonstrated a SST seesaw between the two regions that could be a surface expression of the variability of the NAC.

Furthermore, there is a link between the growth rate of Mingulay corals and the εNd of the CWCs (Fig. 3). Small decreases in the εNd values are often associated with an increase in the reef growth rate (Fig. 3). The sensitivity of corals and coral reefs to abrupt climatic and oceanic changes has been pointed out in previous studies (Dodds et al., 2007; Davies et al., 2008; Eisele et al., 2011; Frank et al., 2011; Thiagarajan et al., 2013; Henry et al., 2014; Hebbeln et al., 2014; Douarin et al., 2014; Bonneau et al., 2018). This suggests that the Mingulay Reef Complex is very sensitive to the origin of the water mass. A higher contribution of water originating from the strongly ventilated SPG (such as that observed around 2.8 ka) could cause favorable conditions for CWC growth. Further investigation will be necessary to explain this relationship between changes in the origin of the water masses and coral growth on the Mingulay reef.

6. Conclusion

εNd of seawater and cold-water coral (CWC) samples, collected at depths of 127-134 m in the Mingulay Reef Complex on the Scottish continental shelf, have been investigated in order to constrain subpolar gyre (SPG) dynamics over the past 4500 years.

εNd values obtained in the upper 30 m water depth collected above the Mingulay Reef Complex permit us to establish, for the first time, the surface Nd isotopic signature of the Scottish continental shelf which is around -11.7±0.2, probably due to the influence of radiogenic interior Seas. Below 100 m εNd values vary from -13±0.3 to -12.4±0.2, pointing to a mixing between the Shelf Edge Current (SEC) water and the subpolar water brought by the North Atlantic Current (NAC), as observed in the Porcupine Seabight (Dubois-Dauphin et al., 2017). An influence of the interior Seas cannot be ruled out. In contrast, water station samples collected on the continental slope display unradiogenic εNd values (from -14.4±0.2 to -13.8±0.2), similar to the western Rockall Trough, meaning that NAC water has a strong influence along the continental slope near the study site.

εNd values from the Mingulay Reef Complex show two major variations at 2.8 ka and 3.4 ka, which are synchronous with changes in ^{14}C reservoir age. An unradiogenic εNd value of -14.5±0.4 at 2.8 ka indicated an eastward extension of the SPG associated with a lower ^{14}C reservoir age (200 yrs). Conversely, a more radiogenic value at 3.4 ka (-11.8±0.3) pointed to a stronger northward penetration of the SEC water along the western European margin, combined with a higher ^{14}C reservoir age (600 yrs). The link between εNd and ^{14}C records highlights the fact that ^{14}C reservoir age cannot be used to track water mass origin as it has been previously interpreted (Douarin et al., 2016) but rather vertical ventilations that occurred in the NAC and the SEC.

The major negative excursion at 2.8 ka as well as subtler examples recorded in CWCs are systematically associated with warmer climatic conditions in Northern Europe and the Eastern Norwegian Sea linked to an intensification of the surface limb of the AMOC, as has been

previously observed for the Medieval Climatic Anomaly (Copard et al., 2012). Such hydrological conditions have stimulated the growth rate of the Mingulay Reef Complex.

Acknowledgements

The research leading to this paper received funding from the National Research Agency L-IPSL project (Grant ANR-10-LABX-0018) and the HAMOC project (Grant ANR-13-BS06-0003). We gratefully acknowledge the support provided by Louise Bordier during Nd isotopic composition analyses. We thank the three reviewers for their helpful and insightful comments. We also thank Marc de Batist for his editorial handling of the manuscript.

Data availability

Data related to this article are all available in Tables 1 and 2.

References

Adkins, J.F., Cheng, H., Boyle, E.A., Druffel, E.R.M., Edwards, R.L., 1998. Deep-Sea Coral Evidence for Rapid Change in Ventilation of the Deep North Atlantic 15,400 Years Ago. Science (80-.). 280, 725–728. doi:10.1126/science.280.5364.725

Andersen, M.B., Stirling, C.H., Zimmermann, B., Halliday, A.N., 2010. Precise determination of the open ocean 234U/238U composition. Geochemistry, Geophys. Geosystems 11. doi:10.1029/2010GC003318

Arhan, M., 1990. The North Atlantic Current and Subarctic Intermediate Water. J. Mar. Res. 48, 109–144. doi:10.1357/002224090784984605

Ascough, P.L.L., Cook, G.T.T., Dugmore, A.J.J., 2009. North Atlantic marine 14C reservoir effects: Implications for late-Holocene chronological studies. Quat. Geochronol. 4, 171–180. doi:10.1016/j.quageo.2008.12.002

Berx, B., Payne, M.R., 2017. The Sub-Polar Gyre Index – a community data set for application in fisheries and environment research. Earth Syst. Sci. Data 9, 259–266. doi:10.5194/essd-9-259-2017

Bond, G., Kromer, B., Beer, J., Muscheler, R., Evans, M.N., Showers, W., Hoffmann, S., Lotti-Bond, R., Hajdas, I., Bonani, G., 2001. Persistent Solar Influence on North Atlantic Climate During the Holocene. Science (80-.). 294, 2130–2136. doi:10.1126/science.1065680

Bonneau, L., Colin, C., Pons-Branchu, E., Mienis, F., Tisnérat-Laborde, N., Blamart, D., Elliot, M., Collard, T., Frank, N., Foliot, L., Douville, E. 2018. Imprint of Holocene Climate Variability on Cold-Water Coral Reef Growth at the SW Rockall Trough margin, NE Atlantic. Geochemistry, Geophysics, Geosystems, 19(8), 2437-2452.

Bower, A.S., Le Cann, B., Rossby, T., Zenk, W., Gould, J., Speer, K., Richardson, P.L., Prater, M.D., Zhang, H.-M., 2002. Directly measured mid-depth circulation in the northeastern North Atlantic Ocean. Nature 419, 603–607. doi:10.1038/nature01078

Cage, A.G., Heinemeier, J., Austin, W.E.N., 2006. Marine Radiocarbon Reservoir Ages in Scottish Coastal and Fjordic Waters. Radiocarbon 48, 31–43. doi:10.1017/S0033822200035372

Cage, A.G., Austin, W.E.N., 2010. Marine climate variability during the last millennium: The Loch Sunart record, Scotland, UK. Quat. Sci. Rev. 29, 1633–1647. doi:10.1016/J.QUASCIREV.2010.01.014

Chen, T., Robinson, L.F., Burke, A., Southon, J., Spooner, P., Morris, P.J., Ng, H.C., 2015. Synchronous centennial abrupt events in the ocean and atmosphere during the last deglaciation. Science (80-.). 349, 1537–41. doi:10.1126/science.aac6159Cheng, H., Adkins, J.F., Edwards, R.L., Boyle, E.A., 2000. U-Th dating of deep-sea corals. Geochim. Cosmochim. Acta 64, 2401–2416. doi:10.1016/S0016-7037(99)00422-6

Colin, C., Frank, N., Copard, K., Douville, E., 2010. Neodymium isotopic composition of deep-sea corals from the NE Atlantic: implications for past hydrological changes during the Holocene. Quat. Sci. Rev. 29, 2509–2517. doi:10.1016/j.quascirev.2010.05.012

Copard, K., Colin, C., Douville, E., Freiwald, A., Gudmundsson, G., De Mol, B., Frank, N., 2010. Nd isotopes in deep-sea corals in the North-eastern Atlantic. Quat. Sci. Rev. 29, 2499–2508. doi:10.1016/j.quascirev.2010.05.025

Copard, K., Colin, C., Frank, N., Jeandel, C., Montero-Serrano, J.-C., Reverdin, G., Ferron, B., 2011. Nd isotopic composition of water masses and dilution of the Mediterranean outflow along the southwest European margin. Geochemistry Geophys. Geosystems 12, Q06020. doi:10.1029/2011GC003529

Copard, K., Colin, C., Henderson, G.M., Scholten, J., Douville, E., Sicre, M.-A., Frank, N., 2012. Late Holocene intermediate water variability in the northeastern Atlantic as recorded by deep-sea corals. Earth Planet. Sci. Lett. 313–314, 34–44. doi:10.1016/j.epsl.2011.09.047

Crocket, K.C., Hill, E., Abell, R.E., Johnson, C., Gary, S.F., Brand, T., Hathorne, E.C., 2018. Rare Earth Element Distribution in the NE Atlantic: Evidence for Benthic Sources, Longevity

528 of the Seawater Signal, and Biogeochemical Cycling. Front. Mar. Sci. 5, 147.
529 doi:10.3389/fmars.2018.00147

530 Daniault, N., Mercier, H., Lherminier, P., Sarafanov, A., Falina, A., Zunino, P., Pérez, F.F.,
531 Ríos, A.F., Ferron, B., Huck, T., Thierry, V., Gladyshev, S., 2016. The northern North
532 Atlantic Ocean mean circulation in the early 21st century. Prog. Oceanogr. 146, 142–158.
533 doi:10.1016/J.POCEAN.2016.06.007

534 Davies, A.J., Duineveld, G.C.A., Lavaleye, M.S.S., Bergman, M.J.N., van Haren, H., Roberts,
535 J.M., 2009. Downwelling and deep-water bottom currents as food supply mechanisms to the
536 cold-water coral Lophelia pertusa (Scleractinia) at the Mingulay Reef Complex. Limnol.
537 Oceanogr. 54, 620–629. doi:10.4319/lo.2009.54.2.0620

538 Davies, A.J., Wisshak, M., Orr, J.C., Murray Roberts, J., 2008. Predicting suitable habitat for
539 the cold-water coral Lophelia pertusa (Scleractinia). Deep Sea Res. Part I Oceanogr. Res. Pap.
540 55, 1048–1062. doi:10.1016/J.DSR.2008.04.010

541 Davies, G.R., Gledhill, A., Hawkesworth, C., 1985. Upper crustal recycling in southern
542 Britain: evidence from Nd and Sr isotopes. Earth Planet. Sci. Lett. 75, 1–12.
543 doi:10.1016/0012-821X(85)90045-7

544 de Vernal, A., Hillaire-Marcel, C., 2006. Provincialism in trends and high frequency changes
545 in the northwest North Atlantic during the Holocene. Glob. Planet. Change 54, 263–290.
546 doi:10.1016/J.GLOPLACHA.2006.06.023

547 Dodds, L.A., Roberts, J.M., Taylor, A.C., Marubini, F., 2007. Metabolic tolerance of the cold-
548 water coral Lophelia pertusa (Scleractinia) to temperature and dissolved oxygen change. J.
549 Exp. Mar. Bio. Ecol. 349, 205–214. doi:10.1016/J.JEMBE.2007.05.013

550 Douarin, M., Elliot, M., Noble, S.R., Moreton, S.G., Long, D., Sinclair, D., Henry, L.-A.,
551 Roberts, J.M., 2016. North Atlantic ecosystem sensitivity to Holocene shifts in Meridional
552 Overturning Circulation. Geophys. Res. Lett. 43, 291–298. doi:10.1002/2015GL065999

553 Douarin, M., Elliot, M., Noble, S.R., Sinclair, D.J., Henry, L.-A., Long, D., Moreton, S.G.,
554 Murray Roberts, J., 2013. Growth of north-east Atlantic cold-water coral reefs and mounds
555 during the Holocene: A high resolution U-series and 14C chronology. Earth Planet. Sci. Lett.
556 375, 176–187. doi:10.1016/j.epsl.2013.05.023

557 Douarin, M., Sinclair, D.J., Elliot, M., Henry, L.-A., Long, D., Mitchison, F., Roberts, J.M.,
558 2014. Changes in fossil assemblage in sediment cores from Mingulay Reef Complex (NE
559 Atlantic): Implications for coral reef build-up. Deep Sea Res. Part II Top. Stud. Oceanogr. 99,
560 286–296. doi:10.1016/j.dsr2.2013.07.022

561 Douville, E., Sallé, E., Frank, N., Eisele, M., Pons-Branchu, E., Ayrault, S., 2010. Rapid and
562 accurate U–Th dating of ancient carbonates using inductively coupled plasma-quadrupole
563 mass spectrometry. Chem. Geol. 272, 1–11. doi:10.1016/j.chemgeo.2010.01.007

564 Dubois-Dauphin, Q., Colin, C., Bonneau, L., Montagna, P., Wu, Q., Van Rooij, D., Reverdin,
565 G., Douville, E., Thil, F., Waldner, A., Frank, N., 2017. Fingerprinting Northeast Atlantic
566 water masses using neodymium isotopes. Geochim. Cosmochim. Acta 210, 267–288.
567 doi:10.1016/j.gca.2017.04.002

568 Dubois-Dauphin, Q., Bonneau, L., Colin, C., Montero-Serrano, J.-C.C., Montagna, P.,
569 Blamart, D., Hebbeln, D., Van Rooij, D., Pons-Branchu, E., Hemsing, F., Wefing, A.-M.M.,
570 Frank, N., 2016. South Atlantic intermediate water advances into the North-east Atlantic with
571 reduced Atlantic meridional overturning circulation during the last glacial period.
572 Geochemistry, Geophys. Geosystems 17, 2336–2353. doi:10.1002/2016GC006281

573 Eiríksson, J., Knudsen, K.L., Larsen, G., Olsen, J., Heinemeier, J., Bartels-Jónsdóttir, H.B.,
574 Jiang, H., Ran, L., Símonarson, L.A., 2011. Coupling of palaeoceanographic shifts and
575 changes in marine reservoir ages off North Iceland through the last millennium. Palaeogeogr.
576 Palaeoclimatol. Palaeoecol. 302, 95–108.

577 Eisele, M., Frank, N., Wienberg, C., Hebbeln, D., López Correa, M., Douville, E., Freiwald,
578 A., 2011. Productivity controlled cold-water coral growth periods during the last glacial off
579 Mauritania. Mar. Geol. 280, 143–149. doi:10.1016/j.margeo.2010.12.007

580 Ellett, D.J., Edwards, A., 1983. Oceanography and inshore hydrography of the Inner
581 Hebrides. Proc. R. Soc. Edinburgh. Sect. B. Biol. Sci. 83, 144–160.

582 Ellett, D.J., Edwards, A., Bowers, R., 1986. The hydrography of the Rockall Channel—an
583 overview. Proc. R. Soc. Edinburgh. Sect. B. Biol. Sci. 88, 61–81.
584 doi:10.1017/S0269727000004474

585 Ellett, D.J., Martin, J.H.A., 1973. The physical and chemical oceanography of the Rockall
586 channel. Deep. Res. Oceanogr. Abstr. 20. doi:10.1016/0011-7471(73)90030-2

587 Frank, N., Freiwald, A., López Correa, M., Wienberg, C., Eisele, M., Hebbeln, D., Van Rooij,
588 D., Henriet, J.P., Colin, C., van Weering, T.C.E., de Haas, H., Buhl-Mortensen, P., Roberts,
589 J.M., De Mol, B., Douville, E., Blamart, D., Hatté, C., 2011. Northeastern Atlantic cold-water
590 coral reefs and climate. Geology 39, 743–746. doi:10.1130/G31825.1

591 Franke, J., Paul, A., Schulz, M., 2008. Modeling variations of marine reservoir ages during
592 the last 45 000 years. Clim. Past Discuss. 4, 81–110.

593 Freiwald, A., Fossa, J. H., Grehan, A., Koslow, T., & Roberts, J. M. (2004). Cold water coral
594 reefs: out of sight-no longer out of mind. UNEP-WCMC Biodiversity Series No 22Foukal,
595 N.P., Lozier, M.S., 2017. Assessing variability in the size and strength of the North Atlantic
596 subpolar gyre. J. Geophys. Res. Ocean. 122, 6295–6308. doi:10.1002/2017JC012798

597 Häkkinen, S., Rhines, P.B., Worthen, D.L., 2011. Atmospheric blocking and Atlantic
598 multidecadal ocean variability. Science (80-.). 334, 655–9. doi:10.1126/science.1205683

599 Hall, M.M., Bryden, H.L., 1982. Direct estimates and mechanisms of ocean heat transport.
600 Deep Sea Res. Part A. Oceanogr. Res. Pap. 29, 339–359. doi:10.1016/0198-0149(82)90099-1

Hansen, B., Larsen, K.M.H., Hátún, H., Kristiansen, R., Mortensen, E., Østerhus, S., 2015. Transport of volume, heat, and salt towards the Arctic in the Faroe Current 1993–2013. Ocean Sci. 11, 743–757.

Hansen, B., Østerhus, S., 2000. North Atlantic-Nordic Seas exchanges. Prog. Oceanogr. 45, 109–208. doi:10.1016/S0079-6611(99)00052-X

Hátún, H., Sandø, A.B., Drange, H., Hansen, B., Valdimarsson, H., 2005. Influence of the Atlantic subpolar gyre on the thermohaline circulation. Science (80-.). 309, 1841–1844. doi:10.1126/science.1114777

Hebbeln, D., Wienberg, C., Wintersteller, P., Freiwald, A., Becker, M., Beuck, L., Dullo, C., Eberli, G.P., Glogowski, S., Matos, L., Forster, N., Reyes-Bonilla, H., Taviani, M., 2014. Environmental forcing of the Campeche cold-water coral province, southern Gulf of Mexico. Biogeosciences 11, 1799–1815. doi:10.5194/bg-11-1799-2014

Henry, L.-A., Frank, N., Hebbeln, D., Wienberg, C., Robinson, L., de Flierdt, T. van, Dahl, M., Douarin, M., Morrison, C.L., Correa, M.L., Rogers, A.D., Ruckelshausen, M., Roberts, J.M., 2014. Global ocean conveyor lowers extinction risk in the deep sea. Deep Sea Res. Part I Oceanogr. Res. Pap. 88, 8–16. doi:10.1016/J.DSR.2014.03.004

Hill, A.E., Mitchelson-Jacob, E.G., 1993. Observations of a poleward-flowing saline core on the continental slope west of Scotland. Deep Sea Res. Part I Oceanogr. Res. Pap. 40, 1521–1527.

Hillaire-Marcel, C., de Vernal, A., Bilodeau, G., Weaver, A.J., 2001. Absence of deep-water formation in the Labrador Sea during the last interglacial period. Nature 410, 1073–1077. doi:10.1038/35074059

Hoogakker, B.A.A., Chapman, M.R., McCave, I.N., Hillaire-Marcel, C., Ellison, C.R.W., Hall, I.R., Telford, R.J., 2011. Dynamics of North Atlantic Deep Water masses during the Holocene. Paleoceanography 26. doi:10.1029/2011PA002155

Inall, M., Gillibrand, P., Griffiths, C., MacDougal, N., Blackwell, K., 2009. On the oceanographic variability of the North-West European Shelf to the West of Scotland. J. Mar. Syst. 77, 210–226.

Iorga, M.C., Lozier, M.S., 1999. Signatures of the Mediterranean outflow from a North Atlantic climatology: 2. Diagnostic velocity fields. J. Geophys. Res. Ocean. 104, 26011–26029. doi:10.1029/1999JC900204

Jackson, M.G., Oskarsson, N., Trønnes, R.G., McManus, J.F., Oppo, D.W., Grönvold, K., Hart, S.R., Sachs, J.P., 2005. Holocene loess deposition in Iceland: Evidence for millennial-scale atmosphere-ocean coupling in the North Atlantic. Geology 33, 509–512.

Lacan, F., Jeandel, C., 2005. Acquisition of the neodymium isotopic composition of the North Atlantic Deep Water. Geochemistry Geophys. Geosystems 6, Q12008. doi:10.1029/2005GC000956

Lacan, F., Jeandel, C., 2004. Subpolar Mode Water formation traced by neodymium isotopic composition. Geophys. Res. Lett. 31, L14306. doi:10.1029/2004GL019747

Lacan, F., Jeandel, C., 2001. Tracing Papua New Guinea imprint on the central Equatorial Pacific Ocean using neodymium isotopic compositions and Rare Earth Element patterns. Earth Planet. Sci. Lett. 186, 497–512. doi:10.1016/S0012-821X(01)00263-1

Lambelet, M., van de Flierdt, T., Crocket, K.C., Rehkämper, M., Kreissig, K., Coles, B., Rijkenberg, M.J.A., Gerringa, L.J.A., de Baar, H.J.W., Steinfeldt, R., 2016. Neodymium isotopic composition and concentration in the western North Atlantic Ocean: Results from the GEOTRACES GA02 section. Geochim. Cosmochim. Acta 177, 1–29. doi:10.1016/j.gca.2015.12.019

Larsen, K.M.H., Hátún, H., Hansen, B., Kristiansen, R., 2012. Atlantic water in the Faroe area: sources and variability. ICES J. Mar. Sci. J. du Cons. 69, 802–808.

Lavender, K.L., Brechner Owens, W., Davis, R.E., 2005. The mid-depth circulation of the subpolar North Atlantic Ocean as measured by subsurface floats. Deep. Res. Part I Oceanogr. Res. Pap. 52, 767–785. doi:10.1016/j.dsr.2004.12.007

Lugmair, G.W., Shimamura, T., Lewis, R.S., Anders, E., 1983. Samarium-146 in the Early Solar System: Evidence from Neodymium in the Allende Meteorite. Science (80-.). 222, 1015–1018. doi:10.1126/science.222.4627.1015

Lutringer, A., Blamart, D., Frank, N., Labeyrie, L., 2005. Paleotemperatures from deep-sea corals: scale effects, in: Cold-Water Corals and Ecosystems. Springer-Verlag, Berlin/Heidelberg, pp. 1081–1096. doi:10.1007/3-540-27673-4_54

Mayewski, P. a, Rohling, E.J., Curtstager, J., Karlén, W., Maasch, K., Davidmeeker, L., Meyerson, E., Gasse, F., Vankreveld, S., Holmgren, K., 2004. Holocene climate variability. Quat. Res. 62, 243–255. doi:10.1016/j.yqres.2004.07.001

McCartney, M.S., Mauritzen, C., 2001. On the origin of the warm inflow to the Nordic Seas. Prog. Oceanogr. 51, 125–214. doi:10.1016/S0079-6611(01)00084-2

Miettinen, A., Divine, D., Koç, N., Godtliebsen, F., Hall, I.R., Miettinen, A., Divine, D., Koç, N., Godtliebsen, F., Hall, I.R., 2012. Multicentennial Variability of the Sea Surface Temperature Gradient across the Subpolar North Atlantic over the Last 2.8 kyr. J. Clim. 25, 4205–4219. doi:10.1175/JCLI-D-11-00581.1

Mjell, T.L., Ninnemann, U.S., Eldevik, T., Kleiven, H.K.F., 2015. Holocene multidecadal- to millennial-scale variations in Iceland-Scotland overflow and their relationship to climate. Paleoceanography 30, 558–569. doi:10.1002/2014PA002737

Moffa-Sánchez, P., Hall, I.R., 2017. North Atlantic variability and its links to European climate over the last 3000 years. Nat. Commun. 8, 1726. doi:10.1038/s41467-017-01884-8

Montero-Serrano, J.-C., Frank, N., Colin, C., Wienberg, C., Eisele, M., 2011. The climate influence on the mid-depth Northeast Atlantic gyres viewed by cold-water corals. Geophys. Res. Lett. 38. doi:10.1029/2011GL048733

Montero-Serrano, J.-C., Frank, N., Tisnérat-Laborde, N., Colin, C., Wu, C., Lin, K., Shen, C., Copard, K., Orejas, C., Gori, A., De Mol, L., Van Rooij, D., Reverdin, G., Douville, E., 2013. Decadal changes in the mid-depth water mass dynamic of the Northeastern Atlantic margin (Bay of Biscay). Earth Planet. Sci. Lett. 364, 134–144. doi:10.1016/j.epsl.2013.01.012

New, A.L., Barnard, S., Herrmann, P., Molines, J.M., 2001. On the origin and pathway of the saline inflow to the Nordic Seas: Insights from models. Prog. Oceanogr. 48, 255–287. doi:10.1016/S0079-6611(01)00007-6

New, A.L., Smythe-Wright, D., 2001. Aspects of the circulation in the rockall trough. Cont. Shelf Res. 21, 777–810. doi:10.1016/S0278-4343(00)00113-8

O'brien, S.R., Mayewski, P.A., Meeker, L.D., Meese, D.A., Twickler, M.S., Whitlow, S.I., 1995. Complexity of Holocene climate as reconstructed from a Greenland ice core.

Oppo, D.W., McManus, J.F., Cullen, J.L., 2003. Palaeo-oceanography: Deepwater variability in the Holocene epoch. Nature 422, 277.

Penny Holliday, N., Pollard, R.T., Read, J.F., Leach, H., 2000. Water mass properties and fluxes in the Rockall Trough, 1975-1998. Deep. Res. Part I Oceanogr. Res. Pap. 47, 1303–1332. doi:10.1016/S0967-0637(99)00109-0

Pollard, R.T., Griffttths, M.J., Cunningham, S.A., Read, J.F., Pérez, F.F., Ríos, A.F., 1996. Vivaldi 1991 - A study of the formation, circulation and ventilation of Eastern North Atlantic Central Water. Prog. Oceanogr. 37, 167–192. doi:10.1016/S0079-6611(96)00008-0

Read, J.., 2001. CONVEX-91: water masses and circulation of the Northeast Atlantic subpolar gyre. Prog. Oceanogr. 48, 461–510. doi:10.1016/S0079-6611(01)00011-8

Renssen, H., Seppä, H., Heiri, O., Roche, D.M., Goosse, H., Fichefet, T., 2009. The spatial and temporal complexity of the Holocene thermal maximum. Nat. Geosci. 2, 411–414. doi:10.1038/ngeo513

Roberts, N.L., Piotrowski, A.M., 2015. Radiogenic Nd isotope labeling of the northern NE Atlantic during MIS 2. Earth Planet. Sci. Lett. 423, 125–133. doi:10.1016/j.epsl.2015.05.011

Sabatier, P., Reyss, J.-L., Hall-Spencer, J.M., Colin, C., Frank, N., Tisnérat-Laborde, N., Bordier, L., Douville, E., 2012a. 210Pb-226Ra chronology reveals rapid growth rate of Madrepora oculata and Lophelia pertusa on world's largest cold-water coral reef. Biogeosciences 9, 1253–1265. doi:10.5194/bg-9-1253-2012

Sabatier, P., Dezileau, L., Colin, C., Briqueu, L., Bouchette, F., Martinez, P., Siani, G., Raynal, O., Von Grafenstein, U., 2012b. 7000years of paleostorm activity in the NW Mediterranean Sea in response to Holocene climate events. Quat. Res. 77, 1–11.

Sicre, M.-A., Yiou, P., Eiríksson, J., Ezat, U., Guimbaut, E., Dahhaoui, I., Knudsen, K.L., Jansen, E., Turon, J.L., 2008. A 4500-year reconstruction of sea surface temperature variability at decadal time-scales off North Iceland. Quat. Sci. Rev. 27, 2041–2047. doi:10.1016/j.quascirev.2008.08.009

Sorrel, P., Debret, M., Billeaud, I., Jaccard, S.L., McManus, J.F., Tessier, B., 2012. Persistent non-solar forcing of Holocene storm dynamics in coastal sedimentary archives. Nat. Geosci. 5, 892–896. doi:10.1038/ngeo1619

Stewart, H.A., Gatliff, R.W., 2008. Preliminary geological results of sea-bed sampling in the Hebrides area from the RRS James Cook in 2007.

Struve, T., van de Flierdt, T., Burke, A., Robinson, L.F., Hammond, S.J., Crocket, K.C., Bradtmiller, L.I., Auro, M.E., Mohamed, K.J., White, N.J., 2017. Neodymium isotopes and concentrations in aragonitic scleractinian cold-water coral skeletons - Modern calibration and evaluation of palaeo-applications. Chem. Geol. 453, 146–168. doi:10.1016/j.chemgeo.2017.01.022

Stuiver, M., Reimer, P.J., Braziunas, T.F., 1998. High-Precision Radiocarbon Age Calibration for Terrestrial and Marine Samples. Radiocarbon 40, 1127–1151. doi:10.2458/azu_js_rc.v40i3.3786

Stuiver, M., Braziunas, T.F., 1993. Modeling Atmospheric 14C Influences and 14C Ages of Marine Samples to 10,000 BC. Radiocarbon 35, 137–189. doi:10.1017/S0033822200013874

Tanaka, T., Togashi, S., Kamioka, H., Amakawa, H., Kagami, H., Hamamoto, T., Yuhara, M., Orihashi, Y., Yoneda, S., Shimizu, H., Kunimaru, T., Takahashi, K., Yanagi, T., Nakano, T., Fujimaki, H., Shinjo, R., Asahara, Y., Tanimizu, M., Dragusanu, C., 2000. JNdi-1: a neodymium isotopic reference in consistency with LaJolla neodymium. Chem. Geol. 168, 279–281. doi:10.1016/S0009-2541(00)00198-4

Thornalley, D.J.R., Blaschek, M., Davies, F.J., Praetorius, S., Oppo, D.W., McManus, J.F., Hall, I.R., Kleiven, H., Renssen, H., McCave, I.N., 2013. Long-term variations in Iceland–Scotland overflow strength during the Holocene. Clim. Past 9, 2073–2084. doi:10.5194/cp-9-2073-2013

Thornalley, D.J.R., Elderfield, H., McCave, I.N., 2009. Holocene oscillations in temperature and salinity of the surface subpolar North Atlantic. Nature 457, 711–4. doi:10.1038/nature07717

Tisnérat-Laborde, N., Paterne, M., Métivier, B., Arnold, M., Yiou, P., Blamart, D., Raynaud, S., 2010. Variability of the northeast Atlantic sea surface Δ 14 C and marine reservoir age and the North Atlantic Oscillation (NAO). Quat. Sci. Rev. 29, 2633–2646.

van de Flierdt, T., Pahnke, K., Amakawa, H., Andersson, P., Basak, C., Coles, B., Colin, C., Crocket, K.C., Frank, M., Frank, N., 2012. GEOTRACES intercalibration of neodymium isotopes and rare earth element concentrations in seawater and suspended particles. Part 1: reproducibility of results for the international intercomparison. Limnol. Oceanogr. Methods 10, 234–251. doi:10.4319/lom.2012.10.234

van de Flierdt, T., Robinson, L.F., Adkins, J.F., 2010. Deep-sea coral aragonite as a recorder for the neodymium isotopic composition of seawater. Geochim. Cosmochim. Acta 74, 6014–6032. doi:10.1016/j.gca.2010.08.001

751 Wanamaker Jr, A.D., Butler, P.G., Scourse, J.D., Heinemeier, J., Eiríksson, J., Knudsen, K.L.,
752 Richardson, C.A., 2012. Surface changes in the North Atlantic meridional overturning
753 circulation during the last millennium. Nat. Commun. 3, 899.

754 White, M., Bowyer, P., 1997. The shelf-edge current north-west of Ireland. Ann. Geophys.
755 15, 1076–1083. doi:10.1007/s00585-997-1076-0

756 Wilson, D.J., Crocket, K.C., van de Flierdt, T., Robinson, L.F., Adkins, J.F., 2014. Dynamic
757 intermediate ocean circulation in the North Atlantic during Heinrich Stadial 1: A radiocarbon
758 and neodymium isotope perspective. Paleoceanography 29, 1072–1093.
759 doi:10.1002/2014PA002674

760 Wu, Q., Colin, C., Liu, Z., Douville, E., Dubois-Dauphin, Q., Frank, N., 2015. New insights
761 into hydrological exchange between the South China Sea and the Western Pacific Ocean
762 based on the Nd isotopic composition of seawater. Deep Sea Res. Part II 122, 1–16.
763 doi:10.1016/j.dsr2.2015.11.005

764 Zunino, P., Lherminier, P., Mercier, H., Daniault, N., García-Ibáñez, M.I., Pérez, F.F., 2017.
765 The GEOVIDE cruise in May–June 2014 reveals an intense Meridional Overturning
766 Circulation over a cold and fresh subpolar North Atlantic. Biogeosciences 14, 5323–5342.
767 doi:10.5194/bg-14-5323-2017

768

769 **Figure captions**

770 **Fig. 1.** Sampling map. The schematic circulations of surface currents are reported by black
771 arrows based on Daniault et al. (2016) and Cage & Austin (2010). NAC, North Atlantic
772 Current; SCC, Scottish Coastal Current; SEC, Shelf Edge Current; SPG, Subpolar Gyre; STG,
773 Subtropical Gyre. Seawater εNd values at 100-150m (in white) have been reported from
774 Dubois-Dauphin et al. (2017) and Lambelet et al. (2016). The location of CWCs investigated
775 by Colin et al. (2010) and Copard et al. (2012) in the Rockall Trough are indicated by a green
776 square. Marine cores discussed in the text are indicated by black dots: a. MD99-2275 (Sicre
777 et al., 2008); b. RAPiD-12-1K (Thornalley et al., 2009); c. VM29-191 and d. MC52 (Bond et
778 al., 2001). Water stations are indicated by open dots: e. ICE-CTD 03 (Dubois-Dauphin et al.,
779 2017); f. ICE-CTD 02 (Dubois-Dauphin et al., 2017); g. Carols Stations (Copard et al., 2011);
780 h. Station 9G (Crocket et al., 2018). Seawater stations MR-4 (orange dot, continental slope)

781 and MR-5 (blue dot, continental shelf) investigated in this study are reported on the insert
782 map. The Mingulay Reef Complex is indicated by a red square.

783 **Fig. 2.** Potential temperature (°C), salinity and εNd value depth profiles for stations MR-4
784 (continental slope) and MR-5 (continental shelf).

785 **Fig. 3**. (a) Marine Reservoir Effect (MRE) reconstructed from Mingulay Reef Complex
786 CWCs (Douarin et al., 2016); (b) εNd record from the Mingulay Reef Complex CWCs (blue
787 dots, this study) and from the Rockall Trough (green squares, Colin et al., 2010; Copard et al.,
788 2012). The blue star corresponds to the present day εNd value for station MR-5 at depth of the
789 Mingulay CWCs. The green star corresponds to the present day εNd value for station ICE-
790 CTD 03 (Dubois-Dauphin et al., 2017) at depth of the Rockall CWCs. (c) Reef growth rates
791 estimated from downcore +56-08/930VE (pink) and downcore +56-08/929VE (orange) U-
792 series chronologies; grey dots indicate ages for seabed surface Lophelia dated by radiocarbon
793 and/or U-series (Douarin et al., 2013).

794 **Fig. 4**. Seawater εNd profiles for stations MR-4 and MR-5 compared with previous ones
795 published for the Rockall Trough and the Porcupine Seabight (Dubois-Dauphin et al., 2017),
796 as well as for the Bay of Biscay (Copard et al., 2011)

797 **Fig. 5**. Crossplot of MRE (Douarin et al., 2016) versus εNd (this study) of the Mingulay Reef
798 Complex.

799 **Fig. 6.** (a) High resolution Sea surface temperature (in °C) derived from alkenone
800 paleothermometry (MD99-2275; Sicre et al., 2008). Temporal resolution of the blue curve
801 ranges from 2 to 5 years. The superimposed red curve is a 5 points running mean; (b) εNd
802 record from the Mingulay Reef Complex CWCs (blue dots, this study) and from the Rockall
803 Trough (green squares, Colin et al., 2010; Copard et al., 2012) (c) MRE reconstructed from
804 Mingulay Reef Complex CWCs (Douarin et al., 2016); (d) Sea surface temperatures at surface

805 (red line) and at thermocline level (blue line) (RAPiD12-1K ; Thornalley et al., 2009).(e)
806 Mean grain size (µm) measured in south Icelandic loess (Jackson et al., 2005). (f) Greenland
807 Ice Sheet Project 2 sea-salt sodium as a proxy of westerly winds (O'Brien et al., 1995). MCA:
808 Medieval Climatic Anomaly. Dashed lines underline warm events in North Iceland.

809 **Fig. 7**. Schematic representations of the dynamic of sub-surface circulation in the North
810 Atlantic during the 2.8 event (a) and 3.4 event (b).

811 **Table 1.** εNd values obtained for cold-water corals from the Mingulay Reef Complex.
812 Internal error (2 SE) corresponds to error measurement based on 90 cycles of measurements.
813 External error (2 SD) corresponds to external reproducibility (2σ standard deviation) derived
814 from repeated measurements of La Jolla standard for each analytical session. When internal
815 error is larger than external error, internal error is used in the figures.

816 **Table 2.** Locations, water depth (m), potential temperature (θ, °C), salinity (psu), potential
817 density (σ, kg.m-3), $^{143}Nd/^{144}Nd$ and εNd values of seawater samples investigated in this
818 study. Error bars reported for εNd values correspond to external reproducibility (2σ standard
819 deviation) derived from repeated measurements of La Jolla standard for each analytical
820 session.

821

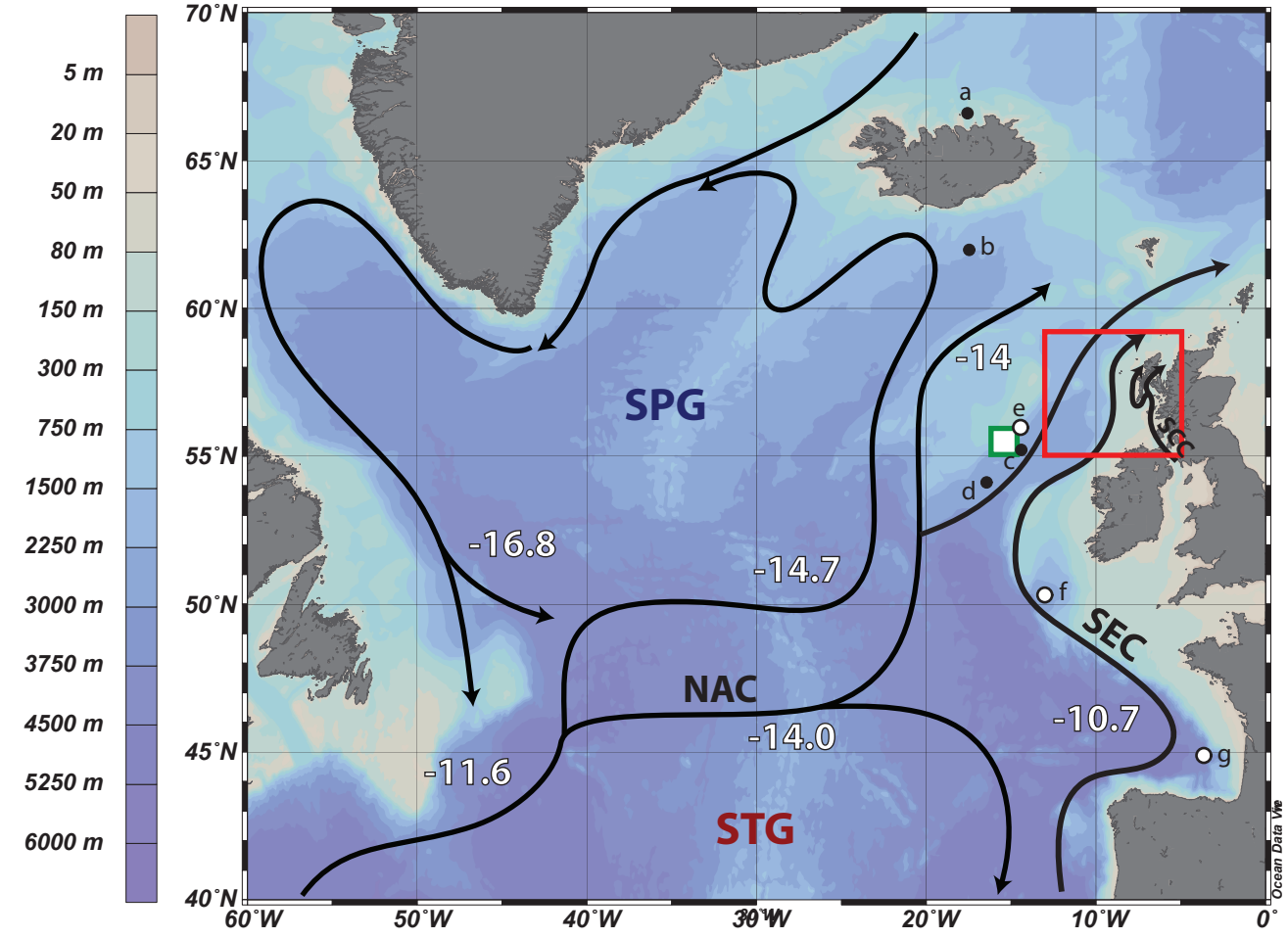
5 m
20 m
50 m
80 m
150 m
300 m
750 m
1500 m
2250 m
3000 m
3750 m
4500 m
5250 m
6000 m
70˚N
65˚N
60˚N
55˚N
50˚N
45˚N
40˚N
60˚W
50˚W
40˚W
30˚W
20˚W
10˚W
0˚
a
b
c
d
e
f
g
SPG
NAC
STG
SEC
SCC
-14
-16.8
-14.7
-14.0
-11.6
-10.7
Ocean Data Vie

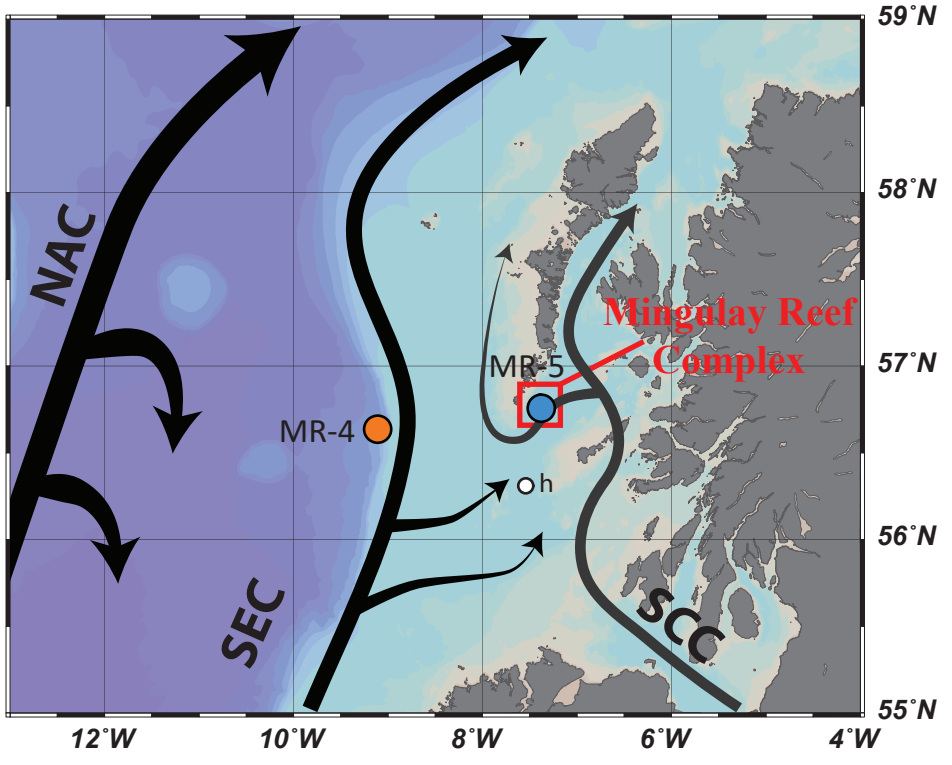
59˚N
58˚N
57˚N
56˚N
55˚N
12˚W
10˚W
8˚W
6˚W
4˚W
NAC
SEC
SCC
MR-4
MR-5
h
Mingulay Reef
Complex

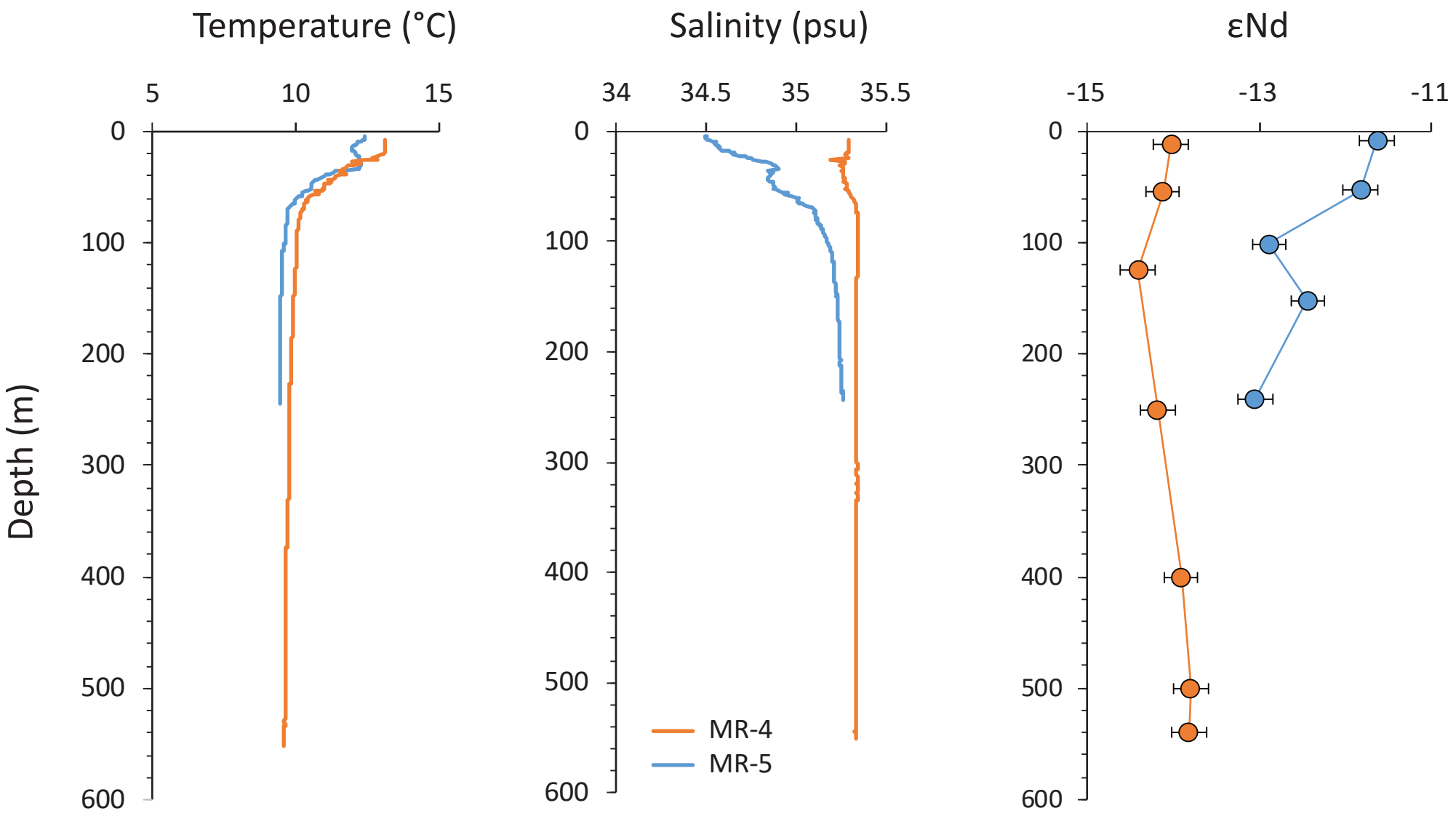
Temperature (°C)
Salinity (psu)
εNd
Depth (m)
5
10
15
34
34.5
35
35.5
-15
-13
-11
0
100
200
300
400
500
600
MR-4
MR-5

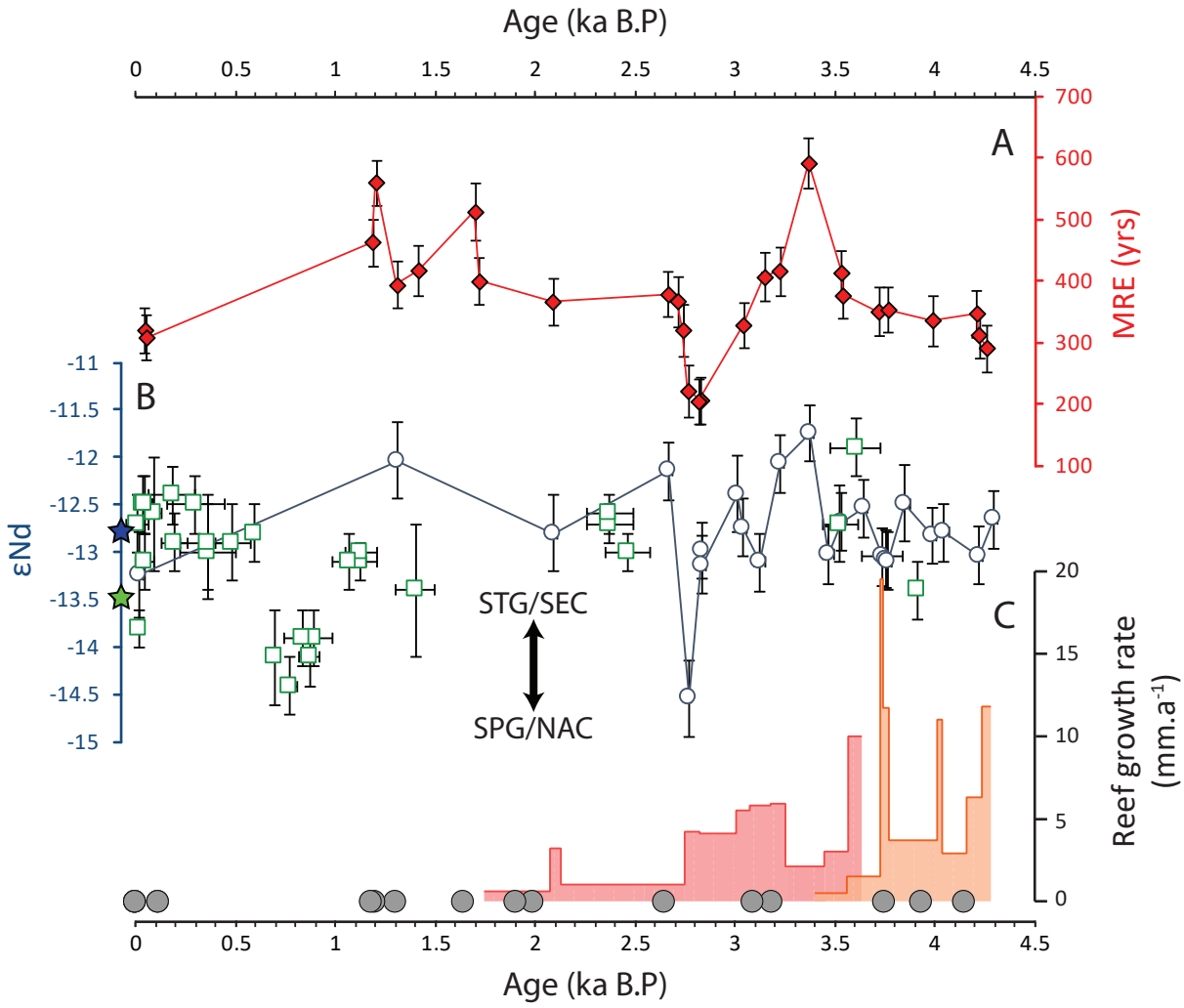
Age (ka B.P)
0
0.5
1
1.5
2
2.5
3
3.5
4
4.5
A
700
600
500
400
300
200
100
MRE (yrs)
B
-11
-11.5
-12
-12.5
-13
-13.5
-14
-14.5
-15
εNd
STG/SEC
SPG/NAC
C
20
15
10
5
0
Reef growth rate
(mm.a-1)
Age (ka B.P)

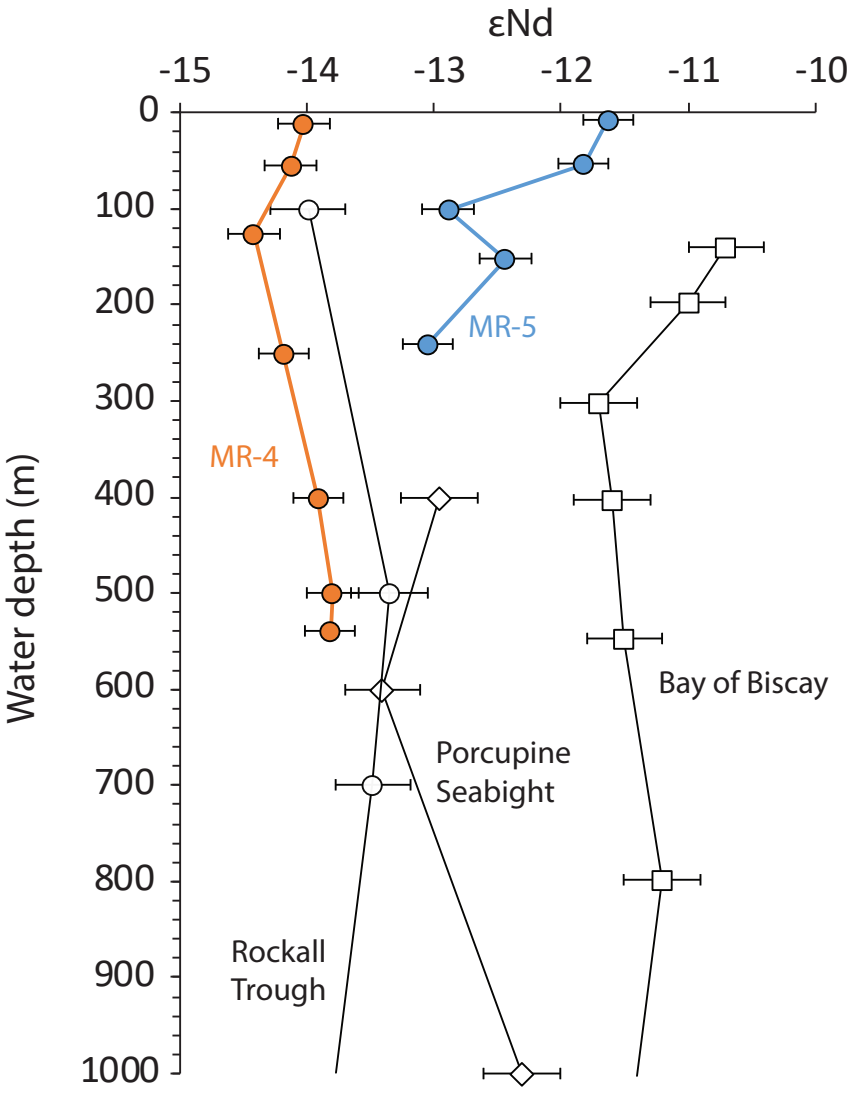
εNd
-15
-14
-13
-12
-11
-10
0
100
200
300
400
500
600
700
800
900
1000
Water depth (m)
MR-4
MR-5
Bay of Biscay
Porcupine
Seabight
Rockall
Trough

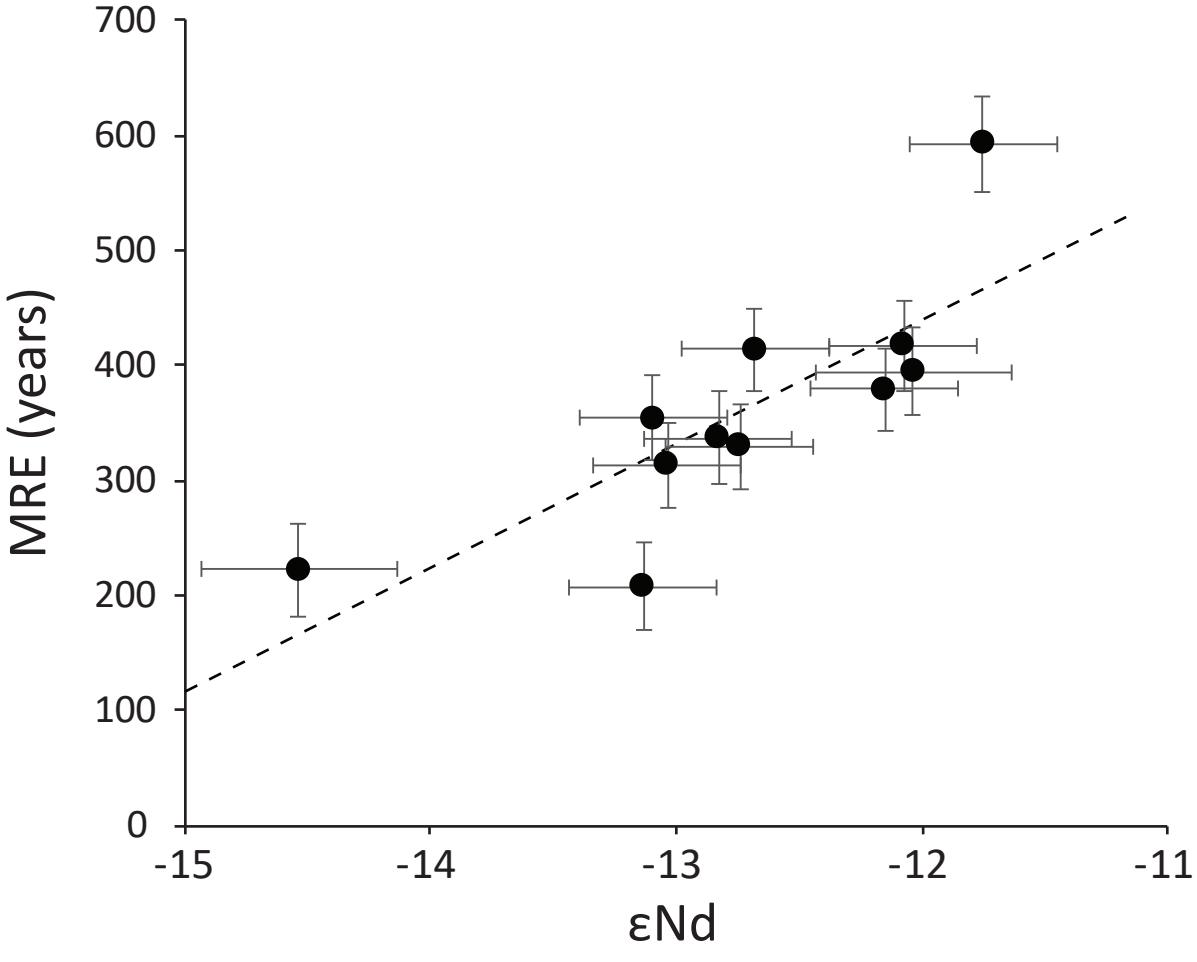
700
600
500
400
300
200
100
0
MRE (years)
-15
-14
-13
-12
-11
εNd

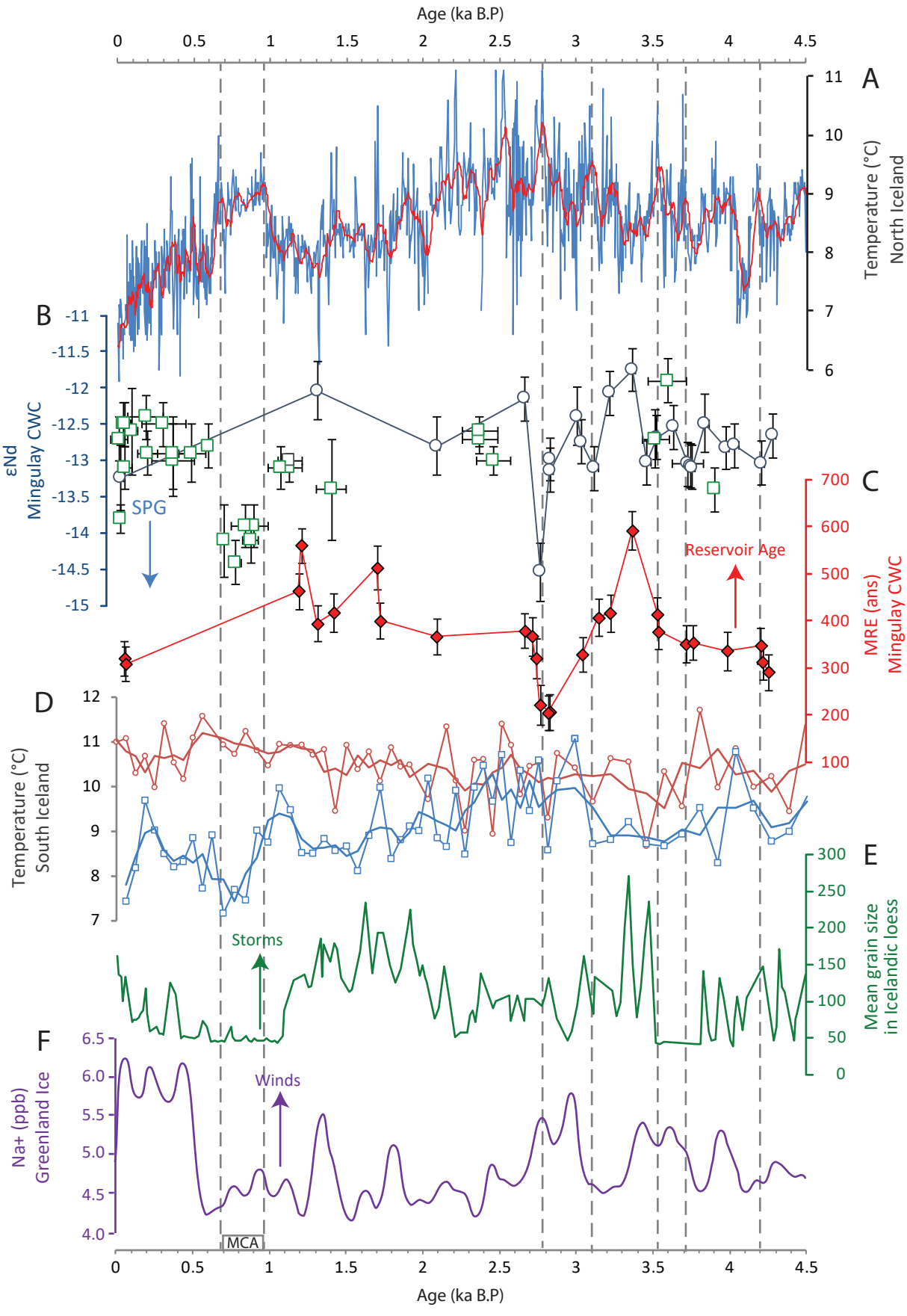
Age (ka B.P)
0
0.5
1
1.5
2
2.5
3
3.5
4
4.5
A
Temperature (°C)
North Iceland
11
10
9
8
7
6
B
εNd
Mingulay CWC
-11
-11.5
-12
-12.5
-13
-13.5
-14
-14.5
-15
SPG
C
MRE (ans)
Mingulay CWC
700
600
500
400
300
200
100
Reservoir Age
D
Temperature (°C)
South Iceland
12
11
10
9
8
7
E
Mean grain size
in Icelandic loess
300
250
200
150
100
50
0
Storms
F
Na+ (ppb)
Greenland Ice
6.5
6.0
5.5
5.0
4.5
4.0
Winds
MCA
Age (ka B.P)

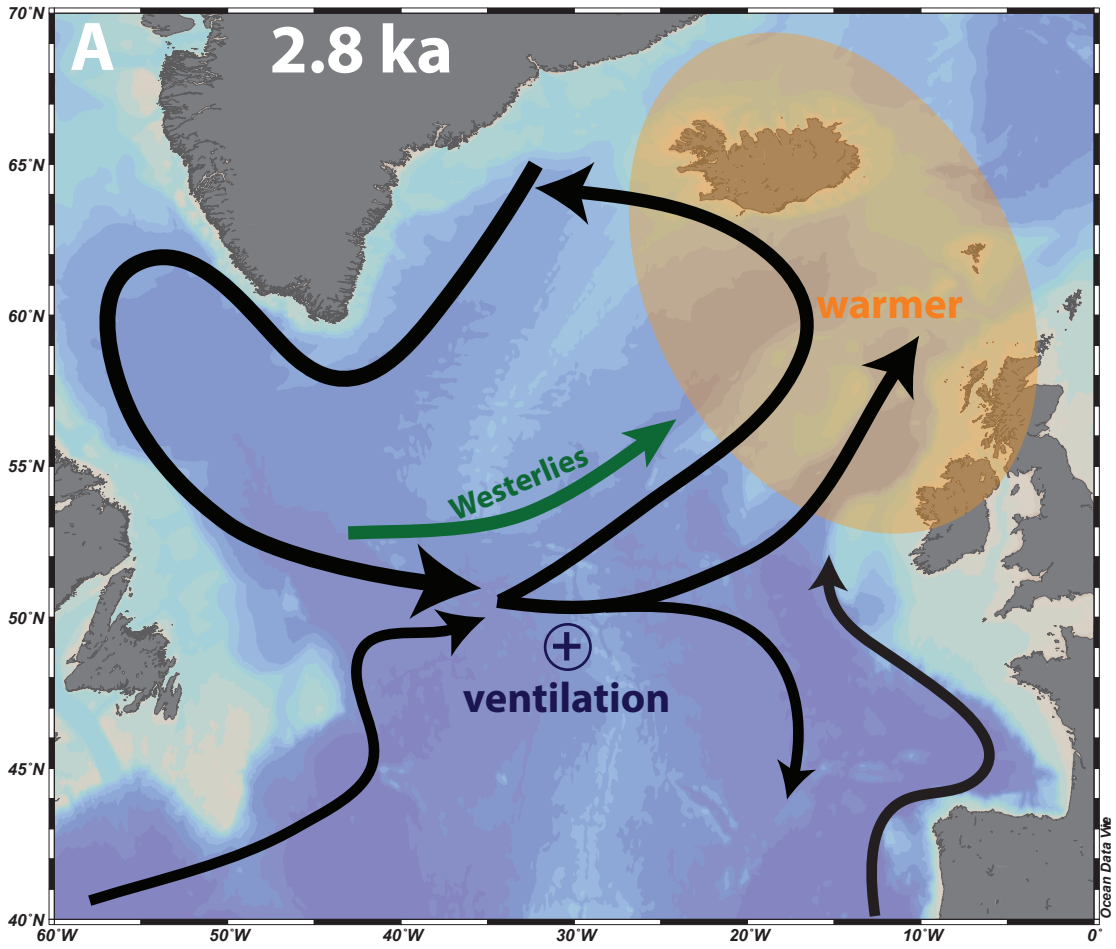
A
2.8 ka
warmer
Westerlies
ventilation
70°N
65°N
60°N
55°N
50°N
45°N
40°N
60°W
50°W
40°W
30°W
20°W
10°W
0°
Ocean Data Vie

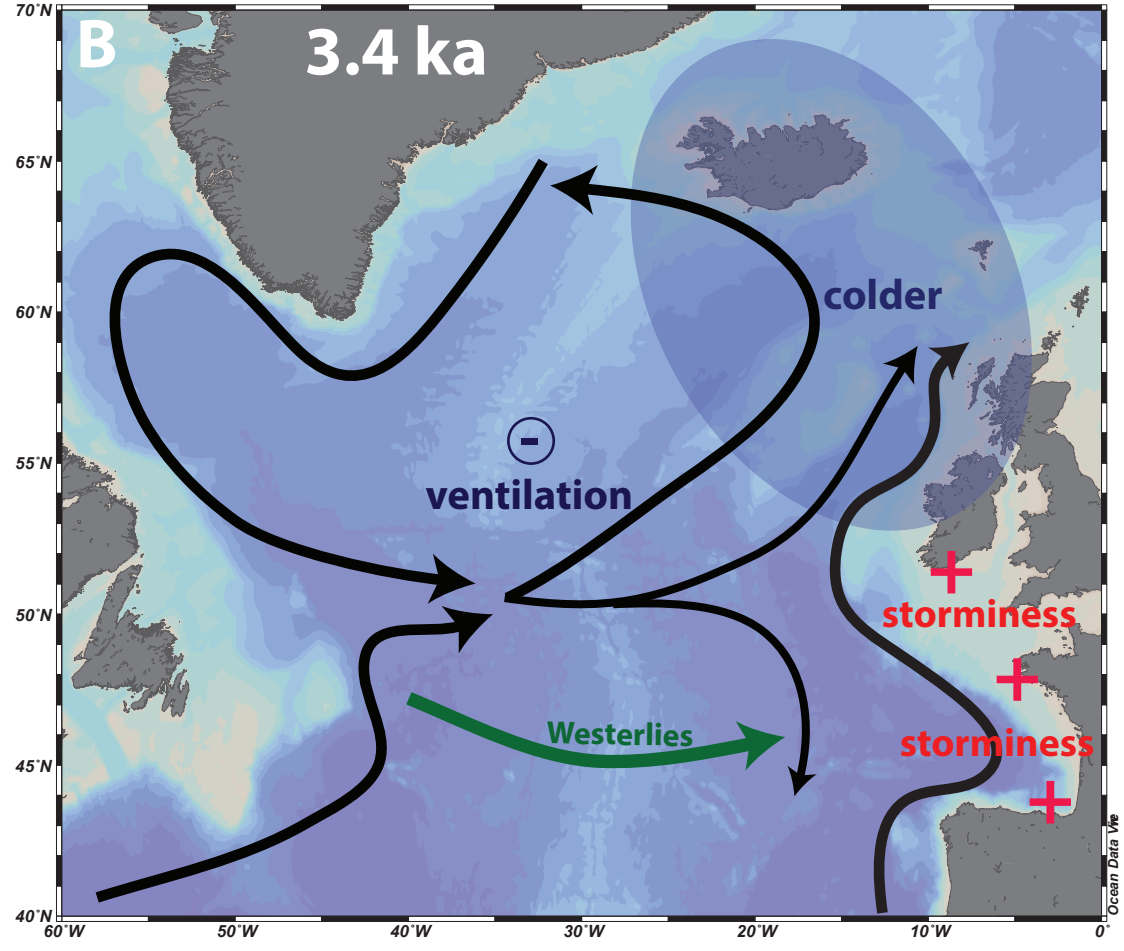
B
3.4 ka
colder
ventilation
Westerlies
storminess
storminess
70°N
65°N
60°N
55°N
50°N
45°N
40°N
60°W
50°W
40°W
30°W
20°W
10°W
0°
Ocean Data Vie

Sample Name	Latitude	Longitude	Depth (m)	Age (yrs)	$^{143}Nd/^{144}Nd$	error (2 SE)	εNd	error (2 SE)	error (2 SD)
GRAB 15.5.5.10	56°47'08" N	7°25'48" W	seafloor	21 ±13	0.511959	±0.000023	-13.24	±0.45	±0.40
GRAB 1151	56°49'08" N	7°23'36" W	seafloor	1312 ±11	0.512021	±0.000021	-12.04	±0.40	±0.40
930 A6 42-45	56°49′20″ N	7°23′47″ W	134	2088 ±18	0.511982	±0.000018	-12.80	±0.36	±0.40
GRAB 56.08.928	56°47'08" N	7°25'48" W	seafloor	2666 ±14	0.512015	±0.000008	-12.15	±0.15	±0.30
930 B6 142-146	56°49′20″ N	7°23′47″ W	134	2765 ±16	0.511893	±0.000021	-14.53	±0.40	±0.40
929 A4 100-101	56°49′19″ N	7°23′27″ W	127	2828 ±13	0.511973	±0.000008	-12.98	±0.15	±0.30
930 B6 134-137	56°49′20″ N	7°23′47″ W	134	2830 ±19	0.511965	±0.000016	-13.13	±0.31	±0.30
930 C6 214-217	56°49′20″ N	7°23′47″ W	134	3012 ±17	0.512003	±0.000018	-12.39	±0.36	±0.40
930 C6 251-254	56°49′20″ N	7°23′47″ W	134	3040 ±11	0.511985	±0.000016	-12.74	±0.31	±0.30
930 D6 388-392	56°49′20″ N	7°23′47″ W	134	3119 ±26	0.511966	±0.000008	-13.11	±0.15	±0.30
930 D6 356-358	56°49′20″ N	7°23′47″ W	134	3221 ±18	0.512019	±0.000012	-12.07	±0.23	±0.30
929 A4 3-9 cm	56°49′19″ N	7°23′27″ W	127	3367 ±18	0.512036	±0.000011	-11.75	±0.21	±0.30
930 D6 377-379	56°49′20″ N	7°23′47″ W	134	3461 ±27	0.511970	±0.000011	-13.03	±0.22	±0.30
929 A4 12-17	56°49′19″ N	7°23′27″ W	127	3530 ±16	0.511988	±0.000008	-12.68	±0.16	±0.30
930 F6 505-510	56°49′20″ N	7°23′47″ W	134	3641 ±22	0.511995	±0.000008	-12.54	±0.15	±0.30
929 A4 38-41	56°49′19″ N	7°23′27″ W	127	3734 ±104	0.511970	±0.000009	-13.04	±0.18	±0.30
929 A4 64-67	56°49′19″ N	7°23′27″ W	127	3747 ±17	0.511968	±0.000015	-13.07	±0.29	±0.30
929 A4 90-91	56°49′19″ N	7°23′27″ W	127	3765 ±13	0.511967	±0.000010	-13.09	±0.19	±0.30
930 E6 459-461	56°49′20″ N	7°23′47″ W	134	3847 ±24	0.511998	±0.000019	-12.49	±0.37	±0.40
929 B4 188-189	56°49′19″ N	7°23′27″ W	134	3986 ±18	0.511980	±0.000012	-12.83	±0.24	±0.30
929 C4 213-216	56°49′19″ N	7°23′27″ W	127	4043 ±23	0.511982	±0.000009	-12.79	±0.18	±0.30
929 C4 284-290	56°49′19″ N	7°23′27″ W	127	4216 ±16	0.511970	±0.000010	-13.03	±0.19	±0.30
929 D4 349-353	56°49′19″ N	7°23′27″ W	127	4287 ±26	0.511989	±0.000011	-12.66	±0.22	±0.30

Table 1

Station	Latitude	Longitude	Depth (m)	θ (°C)	S (psu)	σ (kg.m^{-3})	$^{143}Nd/^{144}Nd$	error (2 SD)	εNd	error (2 SD)
MR-4	56°37.44' N	9°5.48'W	12	13.10	35.29	26.60	0.511919	±0.000010	-14.0	±0.20
MR-4	56°37.44' N	9°5.48'W	55	10.78	35.30	27.05	0.511914	±0.000014	-14.1	±0.30
MR-4	56°37.44' N	9°5.48'W	125	9.99	35.34	27.22	0.511899	±0.000011	-14.4	±0.20
MR-4	56°37.44' N	9°5.48'W	250	9.80	35.34	27.25	0.511911	±0.000012	-14.2	±0.20
MR-4	56°37.44' N	9°5.48'W	400	9.65	35.33	27.27	0.511925	±0.000011	-13.9	±0.20
MR-4	56°37.44' N	9°5.48'W	500	9.63	35.33	27.27	0.511931	±0.000011	-13.8	±0.20
MR-4	56°37.44' N	9°5.48'W	540	9.60	35.33	27.28	0.511930	±0.000012	-13.8	±0.20
MR-5	56°46.04' N	7°25.98'W	8	12.33	34.51	26.15	0.512042	±0.000011	-11.6	±0.20
MR-5	56°46.04' N	7°25.98'W	53	10.39	34.89	26.80	0.512032	±0.000011	-11.8	±0.20
MR-5	56°46.04' N	7°25.98'W	101	9.60	35.18	27.16	0.511977	±0.000012	-12.9	±0.20
MR-5	56°46.04' N	7°25.98'W	152	9.47	35.23	27.22	0.512000	±0.000011	-12.4	±0.20
MR-5	56°46.04' N	7°25.98'W	240	9.43	35.26	27.25	0.511969	±0.000014	-13.0	±0.30

Table 2